The Pennsylvania State University

The Graduate School

TRADEOFFS OF ELECTRONICS LIQUID COOLING DESIGN FEATURES

A Thesis in

Mechanical Engineering

by

Joshua Morse

© 2021 Joshua Morse

Submitted in Partial Fulfillment
of the Requirements
for the Degree of

Master of Science

August 2021

The thesis of Joshua Morse was reviewed and approved by the following:

Bladimir Ramos-Alvarado
Assistant Professor of Mechanical Engineering
Thesis Advisor

Stephen P. Lynch
Associate Professor of Mechanical Engineering

Karen Thole
Department Head of Mechanical Engineering

ABSTRACT

As consumer electronics get more complex, the need for innovation in the field of thermal management increases. Products are getting smaller, smarter, faster, and more computationally demanding. These trends cause the products' electronics to get hotter, as well. Hot temperatures trigger electronics overheating, which causes most instances of electronics failure. Thus, cooling the electronics is essential because products which require electronics to function range across all industries, such as automotive, medical, military, electronics, and tech industries. Some specific product examples include data server racks, electric car batteries, jet engines, and heart rate monitoring equipment. All of these electronics require cooling to avoid failure. Liquid cooling is one common method of cooling electronics. This thesis details liquid cooling heat sink design choices and their effects on heat transfer, fluid flow and fabrication cost. This work also explores the design of liquid cooling for a specific electronics industry application: cooling a circuit board designed and manufactured by the electronics company Keysight Technologies. The approach used was to examine the effect on performance and price of three common design features of liquid cooling heat sinks: the header angle, pin fin geometry, and mini channel geometry. Specifically, the effect of diameter and spacing of the pin fin geometry and the effect of length of the mini channel geometry were examined. The methods used were that of numerical CFD simulation using the Ansys Fluent 19.2 software package. The system's geometry was modeled using 3D modeling software and set up for simulation in Ansys Fluent using the appropriate boundary conditions of the physical system. The simulations yielded raw pressure and temperature data, which were processed into a combined heat transfer and hydraulic performance parameter PPTC. Since this was a real-world application to be used for purchasing prototypes, manufacturing cost was considered as well. The manufacturing price was combined with the PPTC parameter to implement a PPTC/$ parameter, using which can allow comparison between each heat sink design. This

examination of manufacturing price is unique because many studies focus solely on technical performance parameters and neglect the price of fabrication. It was found that the cases with the top three PPTC/$ values, in order from highest to lowest, are MCSF-AL (mini channel short fin-aluminum), MCSF (mini channel short fin-copper), and PF1-2 (Pin fin, 1mm diameter, 1mm spacing-copper).

TABLE OF CONTENTS

LIST OF FIGURES v

LIST OF TABLES vi

ACKNOWLEDGEMENTS vii

Chapter 1 Introduction 1

Chapter 2 Literature Review 3

- 2.1 Electronics Cooling Background 3
- 2.2 Thermal Management of Electronics 3
- 2.3 Liquid-Cooled Heat Sinks: Channels and Pin Fins 6
- 2.4 Flow Maldistribution, Header Types and Distributors 11
- 2.5 Nanofluids 14
- 2.6 Literature Review Summary 16

Chapter 3 Thermal Management Problem Descritption, Approach and Methods 17

- 3.1 Problem Description and Approach 17
- 3.2 Modeling Assumptions and Governing Equations 21
- 3.3 Conduction Simulations: Addressing the Complexity of a Multiscale Heat Transfer Problem 23
- 3.4 Boundary Conditions, Operating Conditions, and Properties 25
- 3.5 Performance Evaluation Metrics 25
- 3.6 Mesh Independence 26
- 3.7 Convection Simulation Procedure 28

Chapter 4 Simulation Results and Discussion 30

- 4.1 Header Design 30
- 4.2 Pin Fin Design 34
  - 4.2.1 Pin Fin Varying Spacing: 0.5mm Diameter 34
  - 4.2.2 Pin Fin Varying Spacing: 1mm Diameter 38
  - 4.2.3 Pin Fin Varying Spacing: 1.5mm Diameter 42
  - 4.2.4 Pin Fin Varying Diameter: 1mm Spacing 46
  - 4.2.5 Pin Fin Varying Diameter: 1.5mm Spacing 50
  - 4.2.6 Pin Fin Varying Diameter: 2mm Spacing 54
- 4.3 Channel Design 58
- 4.4 Select Designs with Aluminum 62
- 4.5 Combined Performance Parameter PPTC and PPTC/Dollar 65

Chapter 5 Conclusion 70

- 5.1 Summary and Conclusions 70
- 5.2 Future work 71

References..72

LIST OF FIGURES

Figure **2.1**: Comparisons of heat transfer effectiveness of conventional methods, figure by Murshed et al. [16]. 4

Figure **2.2**: Commercially available air-cooled heat sink, in which a fan blows air over the fins to cool it off. 5

Figure **2.3**: Tuckerman and Pease's microchannel design with channels 57um wide [18]. 7

Figure **2.4**: Different serpentine channel liquid cooling heat sink designs investigated by Al-Neama et al. [20]. 8

Figure **2.5**: Pin fin liquid cooling heat sinks with locally varying pin fin sizes based on hot spots investigated by Lorenzini et al. [35]. 9

Figure **2.6**: Pin fin heat sink prototypes with varying pin sizings and densities by Chiu et al. [36]. 10

Figure **2.7**: Rectangular header design investigated by Saeed et al. [38]. 12

Figure **2.8**: Flow maldistribution in channels resulting from rectangular header design [38] 12

Figure **2.9**: Angled header investigated by Awais et al. [39]. 13

Figure **2.10**: Flow distribution in channels of rectangular header (red) vs. angled header (black) [39]. 13

Figure **2.11**: One distributor network investigated by Ramos-Alvarado et al. [40]. 14

Figure **2.12**: Channel flow distribution resulting from distributor network B at Re=200 [40]. 14

Figure **2.13**: FESEM image of Al2O3 nanoparticles from Sohel et al. [43]. 15

Figure **3.1**: Circuit board assembly and thermal management system investigated in this thesis. 17

Figure **3.2**: Top level view of PF1-15 design. 18

Figure **3.3**: Zoomed in view showing header angle that is varied for first 4 cases (30 degree shown here). 19

Figure **3.4**: Zoomed in view of PF1-15 showing pin fin diameter and edge-to-edge spacing parameters that are varied throughout the different cases. 19

Figure **3.5**: Dimensions of MCLF (mini channel long fin) heat sink. 20

Figure **3.6**: Dimensions of MCSF (mini channel short fin) heat sink. 21

Figure **3.7** Temperature contour results from the conduction simulations. 24

Figure **3.8**: 12.6 million element mesh, successively zoomed in on pin fins. 27

Figure **4.1**: Total thermal conductance vs. mass flow rate for the 30 degree, 50 degree, 70 degree and 90 degree angle header designs. 32

Figure **4.2**: Pressure drop vs. mass flow rate for the 30 degree, 50 degree, 70 degree and 90 degree angle header designs. 32

Figure **4.3**: Total thermal conductance vs. pumping power for the 30 degree, 50 degree, 70 degree and 90 degree angle header designs. 33

Figure **4.4**: Prices for the 30 degree, 50 degree, 70 degree and 90 degree angle metallic plates compatible with the header designs. 33

Figure **4.5**: Total thermal conductance vs. mass flow rate for pin fin heat sink with 0.5mm diameter and 1mm, 1.5mm, and 2mm spacing. 36

Figure **4.6** Pressure drop vs. mass flow rate for pin fin heat sink with 0.5mm diameter and 1mm, 1.5mm, and 2mm spacing. 36

Figure **4.7**: Total thermal conductance vs. pumping power for pin fin heat sink with 0.5mm diameter and 1mm, 1.5mm, and 2mm spacing. 37

Figure **4.8** Prices for pin fin heat sink with 0.5mm diameter and 0.5mm, 1mm, 1.5mm, and 2mm spacing. 37

Figure **4.9**: Total thermal conductance vs. mass flow rate for pin fin heat sink with 1mm diameter and 1mm, 1.5mm, and 2mm spacing. 40

Figure **4.10**: Pressure drop vs. mass flow rate for pin fin heat sink with 1mm diameter and 1mm, 1.5mm, and 2mm spacing. 40

Figure **4.11**: Total thermal conductance vs. pumping power for pin fin heat sink with 1mm diameter and 1mm, 1.5mm, and 2mm spacing. 41

Figure **4.12**: Prices for pin fin heat sink with 1mm diameter and 1mm, 1.5mm, and 2mm spacing. 41

Figure **4.13**: Total thermal conductance vs. mass flow rate for pin fin heat sink with 1.5mm diameter and 1mm, 1.5mm, and 2mm spacing. 44

Figure **4.14**: Pressure drop vs. mass flow rate for pin fin heat sink with 1.5mm diameter and 1mm, 1.5mm, and 2mm spacing. 44

Figure **4.15**: Total thermal conductance vs. pumping power for pin fin heat sink with 1.5mm diameter and 1mm, 1.5mm, and 2mm spacing. 45

Figure **4.17**: Total thermal conductance vs. mass flow rate for pin fin heat sink with 1mm spacing and 0.5mm, 1mm, and 1.5mm diameter. 48

Figure **4.18**: Pressure drop vs. mass flow rate for pin fin heat sink with 1mm spacing and 0.5mm, 1mm, and 1.5mm diameter. 48

Figure **4.19**: Total thermal conductance vs. pumping power for pin fin heat sink with 1mm spacing and 0.5mm, 1mm, and 1.5mm diameter. 49

Figure **4.20**: Prices for pin fin heat sink with 1mm spacing and 0.5mm, 1mm, and 1.5mm diameter. 49

Figure **4.21**: Total thermal conductance vs. mass flow rate for pin fin heat sink with 1.5mm spacing and 0.5mm, 1mm, and 1.5mm diameter. 52

Figure **4.22**: Pressure drop vs. mass flow rate for pin fin heat sink with 1.5mm spacing and 0.5mm, 1mm, and 1.5mm diameter. 52

Figure **4.23**: Total thermal conductance vs. pumping power for pin fin heat sink with 1.5mm spacing and 0.5mm, 1mm, and 1.5mm diameter. 53

Figure **4.24**: Prices for pin fin heat sink with 1.5mm spacing and 0.5mm, 1mm, and 1.5mm diameter. 53

Figure **4.25**: Total thermal conductance vs. mass flow rate for pin fin heat sink with 2mm spacing and 0.5mm, 1mm, and 1.5mm diameter. 56

Figure **4.26**: Pressure drop vs. mass flow rate for pin fin heat sink with 2mm spacing and 0.5mm, 1mm, and 1.5mm diameter. 56

Figure **4.27**: Total thermal conductance vs. pumping power for pin fin heat sink with 2mm spacing and 0.5mm, 1mm, and 1.5mm diameter. 57

Figure **4.28**: Prices for pin fin heat sink with 2mm spacing and 0.5mm, 1mm, and 1.5mm diameter. 57

Figure **4.29**: Total thermal conductance vs. mass flow rate for mini channel heat sink with 1mm spacing and long and short fins. 60

Figure **4.30**: Pressure drop vs. mass flow rate for mini channel heat sink with 1mm spacing and long and short fins. 60

Figure **4.31**: Total thermal conductance vs. pumping power for mini channel heat sink with 1mm spacing and long and short fins. 61

Figure **4.32**: Price for mini channel heat sink with 1mm spacing and long and short fins. 61

Figure **4.33**: Total thermal conductance vs. mass flow rate for heat sink designs PF1-1 and MCSF in copper material compared with aluminum material. 64

Figure **4.34**: Total thermal conductance vs. pumping power for heat sink designs PF1-1 and MCSF in copper material compared with aluminum material. 64

Figure **4.35**: Prices for heat sink designs PF1-1 and MCSF in copper material compared with aluminum material. 65

Figure **4.36**: The best curve fit found for case PF1-1 simulation data. 67

Figure **4.37**: The best curve fit found for case MCLF simulation data. 67

Figure **4.38**: Pumping power thermal conductivity (PPTC), a combined comparison parameter of each case, copper designs in blue and aluminum designs in grey. 69

Figure **4.39**: Pumping power thermal conductivity (PPTC) per dollar, a combined comparison parameter of each case divided by the case's dollar cost, copper designs in blue and aluminum designs in grey. 69

LIST OF TABLES

Table **1**: Material Properties..25

Table **2**: Performance Evaluation Metrics. 26

Table **3**: Mesh Independence Study Results. 27

Table **4**: Pin fin heat sink geometry parameters..29

Table **5**: Mini channel heat sink geometry parameters. 29

Table **6**: Select cases using aluminum. 29

ACKNOWLEDGEMENTS

This thesis was made possible with the essential help and support from many people. First, I would like to thank my professor and thesis advisor Dr. Bladimir Ramos-Alvarado for teaching me and helping in all aspects of the research, from technical to composition. You are an excellent teacher, and it has been an absolute pleasure learning from you and working with you. I would like to thank Dr. Catherine Berdanier for all her help in teaching me technical writing and helping me with thesis writing. I also want to thank Luis Paniaga-Guerra. Thank you, Luis, for teaching me about CFD simulation and always being available to help me when I ran into problems- your help has been essential. I'd like to thank my engineer colleagues at Keysight Technologies for their advice and guidance. Many people at Keysight have supported me, but I want to specifically mention Randall Spagnola, who has been an amazing engineering mentor for me from day one. I'd like to thank my family for their support in listening to my presentations and giving feedback on them. Lastly, I'd like to thank my good friend Lisa Surber for inspiration, support and commiseration during the master's degree process. I owe a huge debt of gratitude to all the individuals mentioned in this section, so once more, emphatically: thank you.

Chapter 1

Introduction

The cooling of devices is ubiquitous in our world today. It is present in all industries of civilization, such as the medical, automotive, aerospace, housing, and electronics industries. Devices like MRI machines, electric cars, rocket engines, air conditioning systems, and high-powered circuit boards all involve specialized thermal management systems. The current thesis focuses on the cooling of electronic circuit boards. Cooling is extremely important with respect to electronics because overheating causes over half of the failures seen in electronic components. Some devices with circuit boards operate in the extreme heat of desert environments; others may need to function in the vast coldness of outer space, while even still others simply operate in a suburban home at room temperature. Since the devices and applications vary so broadly across industries, so too must the thermal management of these electronic devices vary.

The driving factor of electronics cooling can vary as well. Often, thermal management is required to improve reliability of electronics devices and to reduce the frequency of electronic component failure. Other times, safety of handling the electronic device is a driving cooling concern- it will be problematic of an electronic device is too hot for your consumers to touch or causes its users to get burned in the process. Both the factors of reliability and safety of handling require careful attention to the design of thermal management systems- each new circuit board and device brings a new specific thermal design problem with it.

The purpose of this thesis is three-fold. First, to investigate a real-life application of computational fluid dynamics for a heat transfer problem involving a circuit board that has been manufactured and will be used in instruments at Keysight Technologies, as well as to discover the best choice of liquid cooling heat sink design for this Keysight circuit board. Second, to explore

price differences for design choices such as pin size, pin density, and header angle, as well as compares prices of channel designs vs. pin designs, using a fully-fledged CNC machining prototyping company.

An outline of this thesis follows. The thesis is comprised of five chapters. Chapter 2 is the literature review, which goes into depth on the available literature related to cooling electronics and their relation to the current thesis studies. Chapter 3 is the methods section, which describes the set up and methods used for the research in this thesis. Chapter 4 presents the results of the simulations and offers discussion and interpretation of the results. Chapter 5 involves a summary of the thesis, discussion of future work and any concluding remarks.

Chapter 2

Literature Review

2.1 Electronics Cooling Background

Electronics are the backbone on which modern civilization thrives- and all electronics require cooling of some fashion. Cooling on both a system level (such as servers in a rack) and an individual component level (like electronic chips on a printed circuit board) is critical to the function of electronic devices. Increasing temperature adversely affects the reliability and lifetime of electronics. In extreme examples, devices will either malfunction or simply not operate at all [1]. Pedram and Nazarian [2] reported that over 50% of integrated circuit failures are related to thermal problems. Similarly, Khattak and Ali [3] stated that 55% of electronic failures are due to high temperatures. This sensitivity to heat necessitates the design of adequate electronic cooling methods. As markets demand smaller and smarter (i.e. more thermally intensive) electronic products, the need for smaller and more efficient cooling systems arise as well [4]. The following chapter is an overview of the literature investigation used to direct design decisions for the numerical and experimental cases in this thesis.

2.2 Thermal Management of Electronics

Most methods of electronics cooling rely on convection and can be grouped into the categories of passive cooling [5]–[7], active air-cooling [3], [8], [9], active liquid-cooling [10]–

[12], and phase-change cooling [13]–[15]. Each form of cooling has an observed heat flux range which the method can effectively cool [16]. The most basic form of cooling is passive air

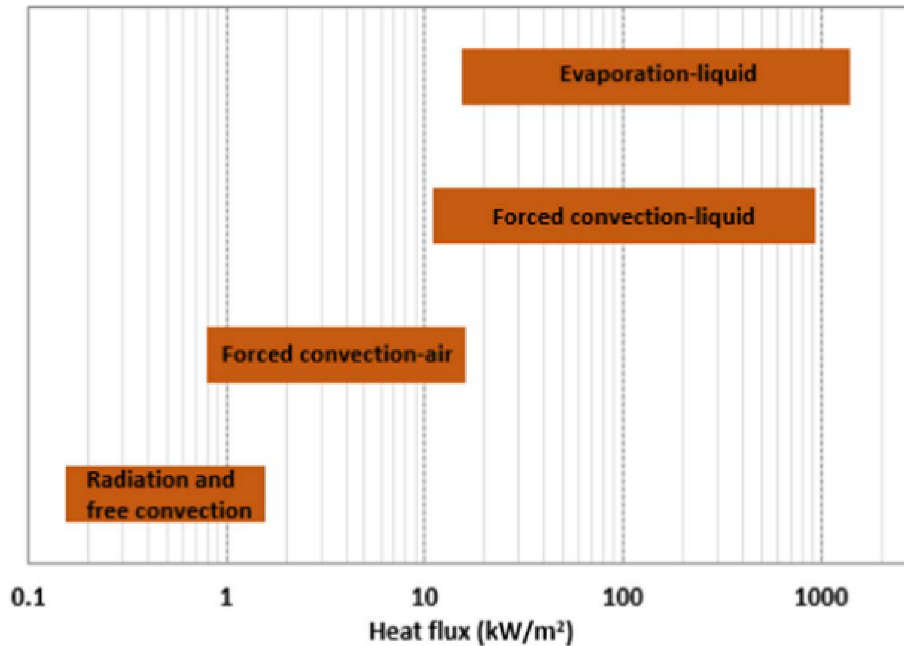

Figure 2.1: Comparisons of heat transfer effectiveness of conventional methods, figure by Murshed et al. [16].

cooling, which involves natural convection: buoyancy induced airflow due to gravitational forces and density stratification over a heat transfer area enhancing device, or heat sink. This type of cooling is simple and cheap, but can only cool low power electronics due to the low heat transfer coefficients obtained through natural convection with gases.

Another common form of cooling is active air-cooling, which involves using a fan to force air across a heat sink. Forced convection air cooling is both simple to implement and cost effective, requiring only a fan and a heat sink. See figure 2.2 for an illustration of this type of heat sink. The simplicity and low cost of forced air cooling cause this method to be one of the most widely used methods in the electronics industry. However, it can only cool a low/mid-tier amount of heat flux from a component or device due to air's low thermal conductivity and the

open-flow nature of air cooling.

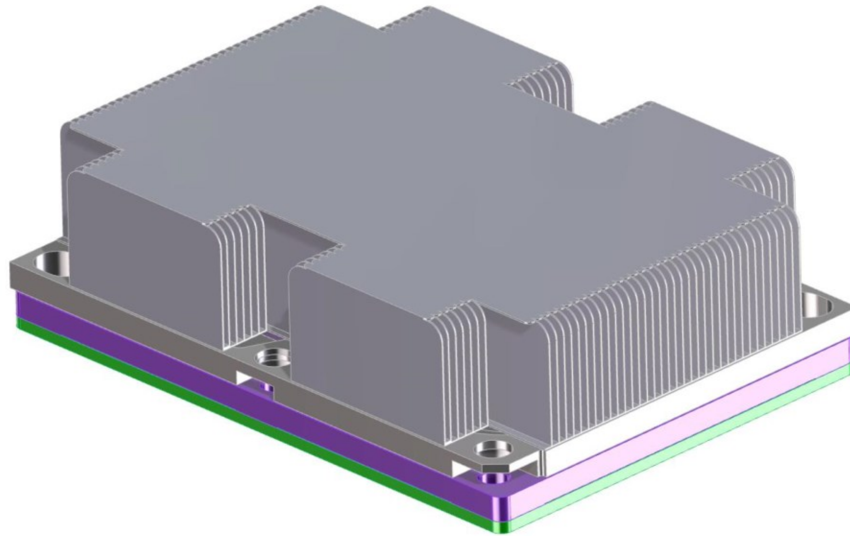

Figure 2.2: Commercially available air-cooled heat sink, in which a fan blows air over the fins to cool it off.

Two-phase liquid cooling, also known as evaporation cooling or flow boiling [17], has received some attention as a viable electronics cooling method. Some main advantages of flow boiling are that it can have very high heat transfer coefficients while keeping liquid flow rates low, as well as allowing good surface temperature uniformity [17]. Two-phase cooling can have an effective heat transfer coefficient of up to 100,000 W/m^2-K, which is impressive compared to single phase liquid cooling's maximum coefficient of 3000 W/m^2-K [16]. Unfortunately flow boiling suffers from problems like flow reversal, flow instability, excess energy waste, and implementation difficulty [13], [15].

Active liquid-cooling maintains an advantage over air cooling in both size (on-circuit-board) and heat transfer efficiency. This method can effectively cool heat fluxes in the range of 10-1000 kW/m^2, while air cooling bottoms out near a limit of 15 kW/m^2 [16]. Thus, the technique of active liquid cooling has been adopted for cooling electronics when other forms of cooling are either not sufficient or are too spatially large.

Between single phase and two phase active liquid cooling, single phase implementation and control is significantly easier than two-phase cooling. To strike a balance between high heat transfer performance and implementation difficulty/cost, the current work focuses on investigating single phase active liquid cooling. Specifically, the research objectives of this thesis are: investigate the monetary tradeoffs of liquid cooling heat sink design features, investigate the fluid dynamic and heat transfer performance tradeoffs of these features, and determine the best design features to cool Keysight Technologies' circuit board when factoring in cost, physical (enclosure space?) constraints, heat transfer and hydrodynamic performance. The following sections explore liquid cooling literature in higher detail, especially with regards to channel heat sinks, pin fin heat sinks, header types, distributor networks and nanofluids.

2.3 Liquid-Cooled Heat Sinks: Channels and Pin Fins

A prevalent form of active liquid-cooling is the implementation of liquid-cooled heat sinks. This design involves cooling by forcing liquid through channels formed by extended surfaces. The extended surfaces increase the wetted surface area compared to flat plate convection, thus increasing the convection heat transfer performance. Liquid micro channel heat sinks (MCHSs) are an increasingly useful route for electronics cooling. The MCHS was first introduced by Tuckerman and Pease [18] in 1981, who showed that heat transfer was improved greatly over conventional liquid cooling channel designs when the designs were scaled down to the micrometer level due to the scaling of the heat transfer coefficient with the hydraulic diameter and the possibility of increasing the density of cooling. Tuckerman and Pease did this using a heat sink that was etched onto the backside of a silicon integrated circuit. Figure 2.1 shows Tuckerman and Pease's microchannel heat sink geometry. Since then, many studies have been done on the

effect of shape and size of channels on hydrodynamic and heat transfer performance [5–7]. For example, Al-Neama et al. [20], using both numerical and experimental methods, applying a

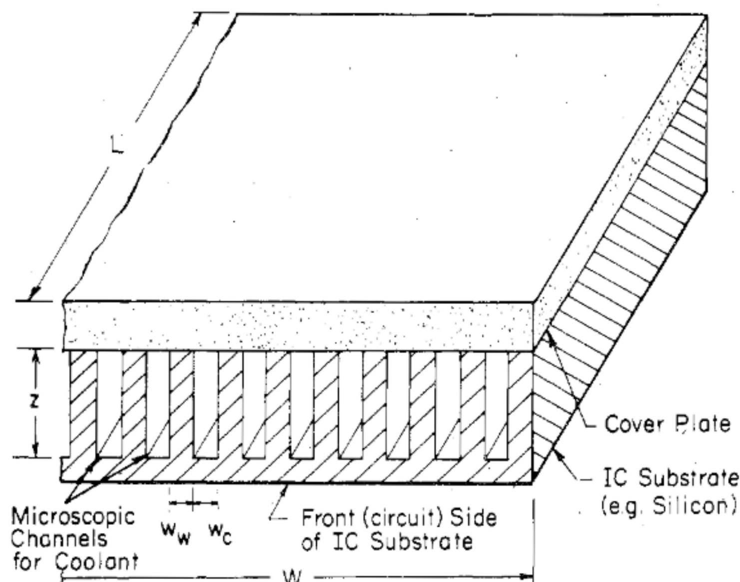

Figure 2.3: Tuckerman and Pease's microchannel design with channels 57um wide [18].

constant heat flux boundary condition or two power film resistors as heat sources respectively, found the single path serpentine microchannel (SPSM) had a 19% reduction in thermal resistance compared to the conventional straight rectangular microchannel (SRM). However, this enhancement is at the expense of a ten-fold increase in pressure drop. Hao et al. [22] used numerical methods to analyze and optimize heat transfer in a channel heat sink whose shape forces the fluid to flow in a U-path. Applying a uniform heat flux to the heat sink, Hao et al. were able to determine the optimal number of channels and channel sizes for best heat transfer and flow distribution in the U-shape heat sink.

Scholars have also extensively studied general improvement techniques of channel liquid cooling, such as surface roughness [23], flow disruptions [12], re-entry obstructions [24], and secondary flows. Increasing surface roughness of channels has been found to reduce thermal resistance, although the roughness becomes detrimental to flow patterns at a certain point [12]. Researchers found that the addition of flow obstructions, such as chevrons [25] or subchannels

[26], reduced both heat sink thermal resistance and pressure drop. Studies also revealed that adding rounded grooves improved heat transfer rate for the heat sink [27]. These studies do great work in revealing different heat transfer enhancement methods, but often neglect discussing the price increase of manufacturing caused by the methods.

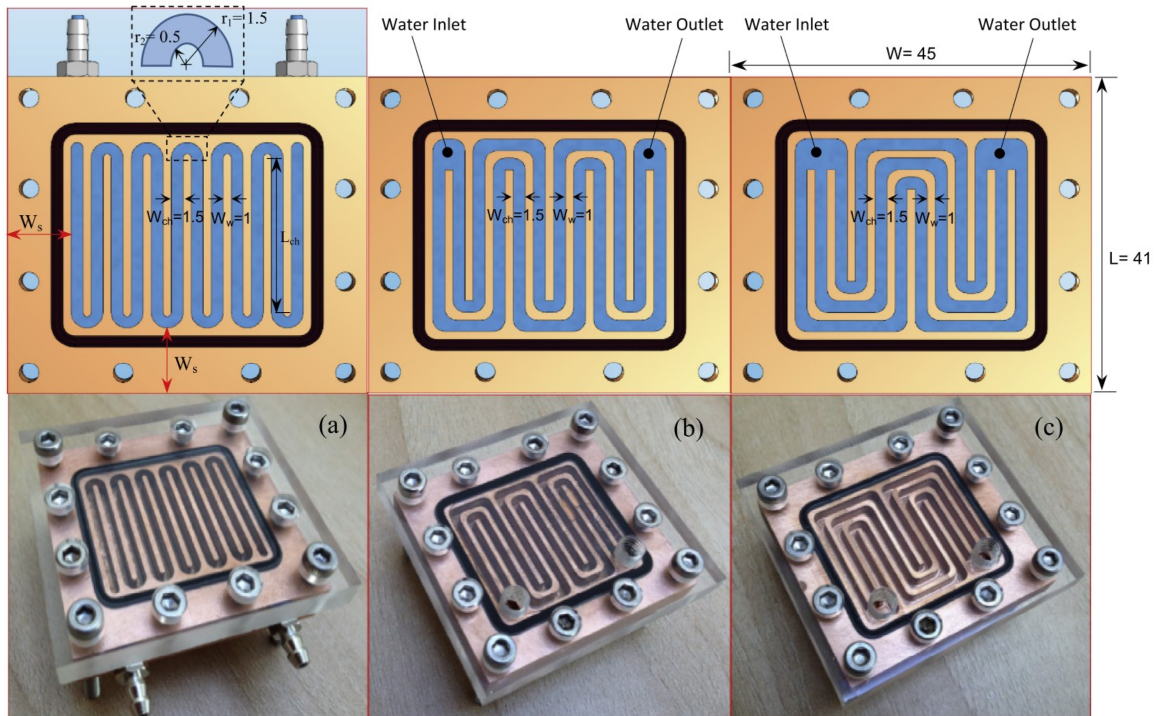

Figure 2.4: Different serpentine channel liquid cooling heat sink designs investigated by Al-Neama et al. [20].

Compared to channel designs, pin fin designs allow a moderate pressure drop while still offering thermal improvements due to the increased wetted surface area. Researchers have performed numerous studies on shape, size, configuration and density of pin fin heat sinks [17–20]. Sahiti et al. [32] found that the optimal shape for pin fins was a hydro-dynamically optimized hydrofoil shape (similar to an airplane wing hydrofoil) which reduced pumping power by 30.4% and improved heat transfer performance by 3.2% over conventional circular pin shapes. The next best pin shape was the circular shape, followed by the rectangular/square shape. Researchers found that staggered pin configurations have improved heat transfer compared to the inline

configurations, but also present a higher pressure drop [33]. Moreover, they found that there exists an optimal fin density at which the thermal resistance of the heat sink begins to increase rather than decrease, and that this fin density depends on the research context [34]. Lorenzini et al. [35] used numerical methods and experiments, implementing platinum RTD heaters as heat sources, to find that varying pin size and density in localized hot spots greatly reduced heat sink thermal resistance while also keeping pressure drop costs down compared to uniformly reducing the pin size and density across the entire heat sink. These results imply that varying pin fin size across a heat sink in a custom cooling solution is beneficial thermally and hydro-dynamically. See figure 2.5 for diagrams of Lorenzini's pin fin liquid cooling heat sinks with locally varying pin fin sizes based on hot spots [35].

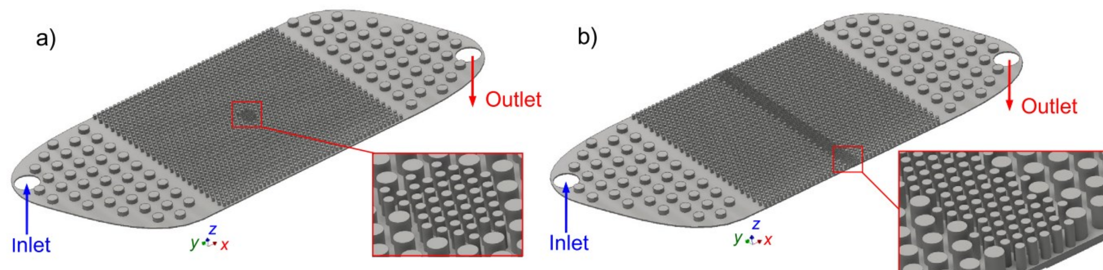

Figure 2.5: Pin fin liquid cooling heat sinks with locally varying pin fin sizes based on hot spots investigated by Lorenzini et al. [35].

Chiu et al. [36] discovered numerically and experimentally, using a resistor as a heat source, that smaller pin diameters provide the best heat transfer for sparse pin fin densities; alternately, they found that for dense pin fin arrays, larger pin diameter works best due to flow rate improvements. See figure 2.6 for two prototype pin fin heat sinks used by Chiu et al [36]. While the heat transfer performance parameters, such as optimal pin shape and spacing, are duly examined and reported in [32]–[36], there is no mention of manufacturing price differences

between the pin configurations; in real-world applications, the cost of fabrication will certainly be

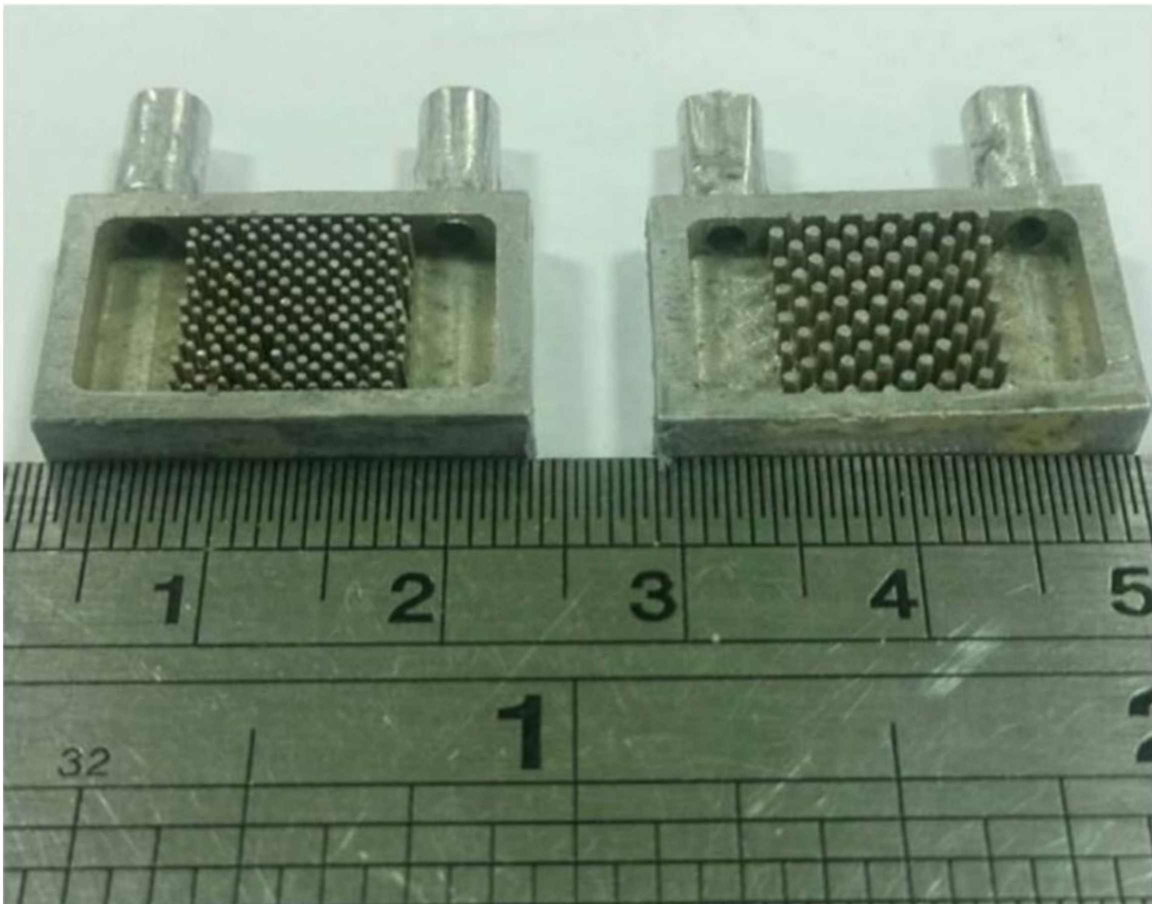

Figure 2.6: Pin fin heat sink prototypes with varying pin sizings and densities by Chiu et al. [36]

a driving design constraint.

Taken as a whole, these studies on liquid cooling do important work in examining heat transfer characteristics, optimizations, and enhancement possibilities in heat sinks. However, the studies on liquid cooling tend to focus on a narrow scope of heat sources. On the experimental side, most of the studies involve cooling single CPU chips or contrived heat sources (i.e. resistor used as heat source). With the numerical investigations, many of the heat source boundary conditions are uniform heat fluxes. These studies are useful to display general heat transfer and fluid flow results, but lack the details of applied engineering to report on data for real life, multi-

chip circuit board heat sources. The current work will find the best design to cool a specific chip configuration on circuit boards made by Keysight Technologies.

As mentioned before, while the plethora of literature on liquid cooling heat sinks do great work in analyzing and reporting on heat transfer and fluid flow optimization, there is little mentioned of fabrication price optimization. In the electronics industry (or any industry for that matter), it is always desirable to find an optimization between performance and price. Since the overarching goal of the current work is to design a heat sink for manufacture and use in the electronics industry, a parallel goal is to report on the cost optimizations and tradeoffs of heat sink design parameters.

2.4 Flow Maldistribution, Header Types and Distributors

One problem in liquid cooled heat sinks is flow maldistribution. Flow maldistribution is when fluid flows at significantly different mass flow and velocity rates throughout the wetted area of the heat sink [37]. This causes unequal cooling and sharp temperature gradients, which are not ideal in cooling electronic chips and devices. This issue is inherent to using single-phase cooling, but it can be mitigated by engineering the flow distribution in function of the heat enhancement features of the heat sink or the location and amgtinude of the heat sources. A heat sink design feature which affects flow maldistribution is the header shape and design. Saeed et al. [38] numerically found that the common rectangular header design caused significant flow maldistribution and had much room for optimization. Figures 2.2 and 2.3 show the rectangular

header design and resulting flow maldistribution investigated by Saeed et al. It can be seen from figure 2.3 that the channels do not have uniform flow velocities.

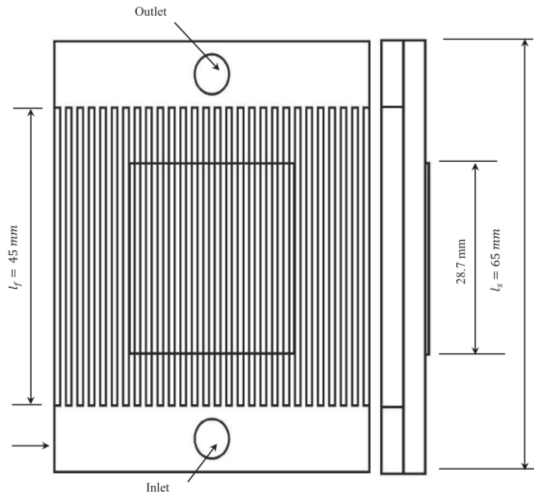

Figure 2.7: Rectangular header design investigated by Saeed et al. [38]

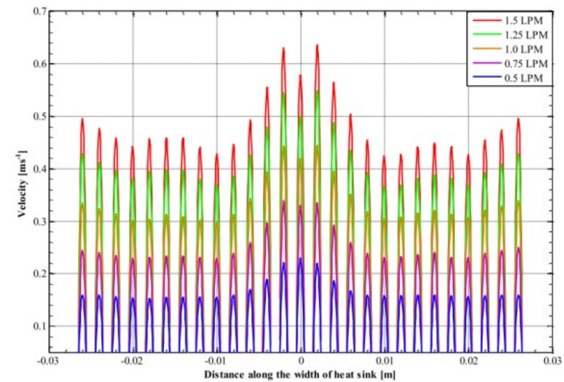

Figure 2.8: Flow maldistribution in channels resulting from rectangular header design [38]

Awais et al. [39] using a mica heater and uniform heat flux respectively, experimentally and numerically found that angled headers perform significantly better than standard rectangular headers. Figures 2.4 and 2.5 show the angled header investigated by Awais et al. and the resulting flow distribution compared to the rectangular header flow distribution. Figure 2.5 shows a dramatic improvement of flow distribution when using the angled header design. Wen et al. [37] numerically studied and proposed a header design that reduces flow maldistribution by incorporating a baffle with varying hole sizes in it.

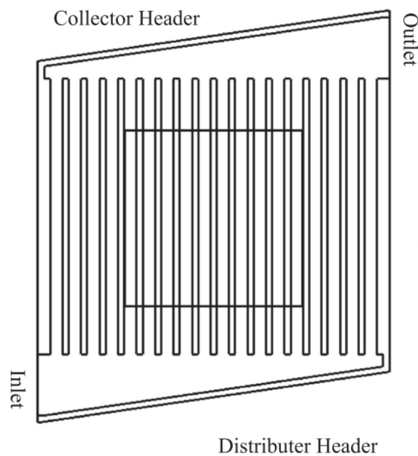

Figure 2.9: Angled header investigated by Awais et al. [39].

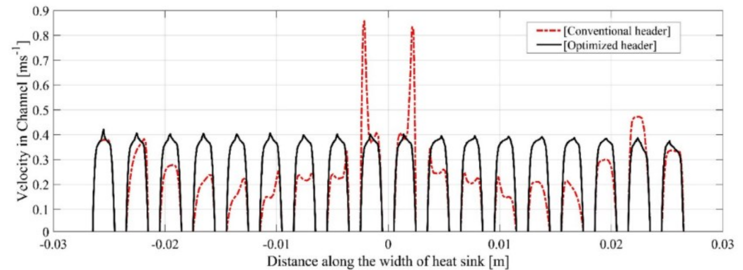

Figure 2.10: Flow distribution in channels of rectangular header (red) vs. angled header (black) [39].

Another way to reduce flow maldistribution is the inclusion of distribution manifolds in the heat sink design. Ramos-Alvarado et al. [40] numerically compared heat sink designs with and without distributor networks and found that conventional heat sink designs had significant flow maldistribution. They also found that the inclusion of distributor networks nearly eradicated flow maldistribution in the channels of the heat sink. Figure 2.11 shows one distributor network design investigated by Ramos-Alvarado et al. Figure 2.12 show's this distributor's effect on flow distribution; the channels all have quite close flow rates.

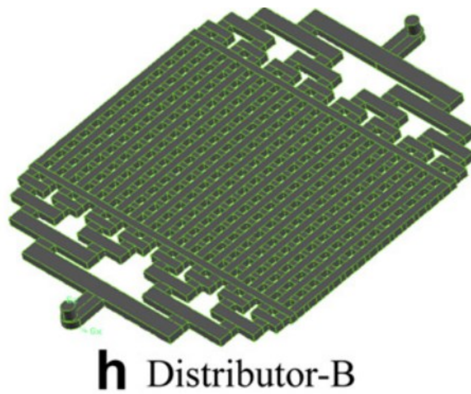

Figure 2.11: One distributor network investigated by Ramos-Alvarado et al. [40].

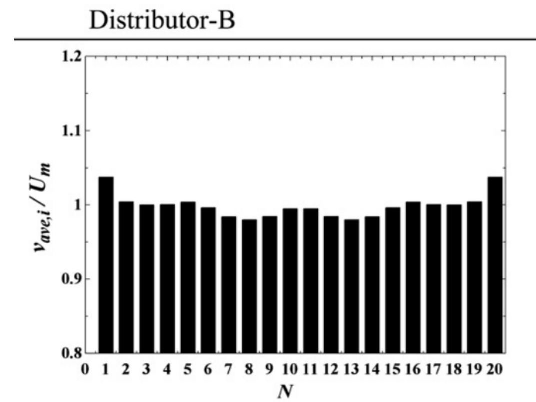

Figure 2.12: Channel flow distribution resulting from distributor network B at Re=200 [40].

Mu et al. [41] numerically investigated standard flow configurations as well as novel flow distributor shapes in liquid cooling heat sinks. They found that both fluid flow and temperature in the heat sinks with standard configurations were poorly distributed. Their novel circular distributor design greatly improved these parameters, lending more evidence that distributor networks improve flow maldistribution and temperature gradients. All these studies on header types and distributor networks contribute to solving the problem of flow maldistribution, but they do not discuss the fabrication cost added by using such features. The current work will take the fabrication cost of header design into account, as well as the metrics of fluid flow and heat transfer performance.

2.5 Nanofluids

Research on nanofluids, small nano-scale particles infused into the working fluid for liquid cooling, has been ongoing for a decade at least [10], [16], [21]. The common parameters that are studied with regards to nanofluids are particle size, concentration and material. These parameters are investigated to determine their effect on heat transfer and fluid flow. Awais et al. [39] numerically and experimentally found that heat transfer capabilities increased with

increasing infusion of aluminum oxide particles **.** See figure 2.13 for a microscopic view of these aluminum oxide particles that the cooling fluid can be suffused with. Similarly, Pryazhnikov et al. [42] found that fluid conductivity increased with larger nano-particle sizes. They also found that the lower the thermal conductivity of the base fluid, the higher the thermal conductivity of the overall nanofluid. Sohel et al. [43], using two cartridge heaters as heat sources, experimentally showed that nanofluids can improve the overall heat transfer coefficient of a liquid cooled microchannel heat sink by 18% over water.

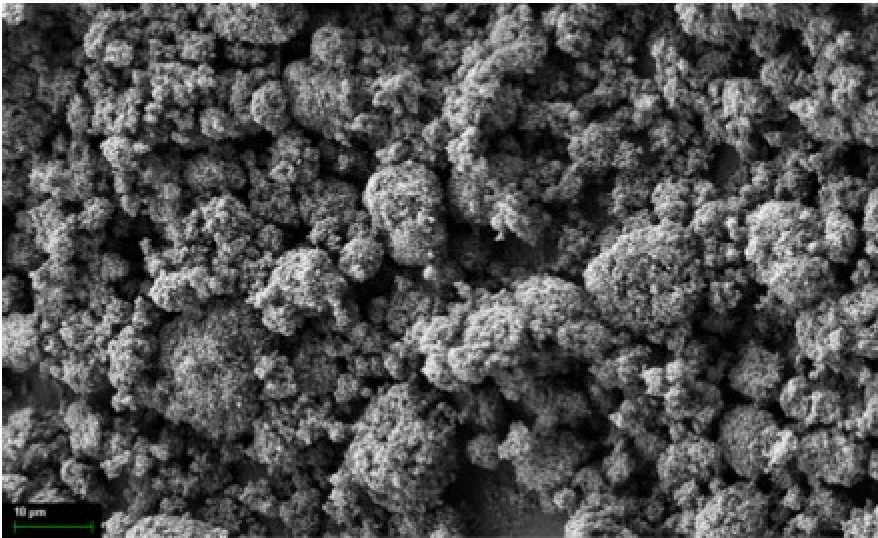

Figure 2.13: FESEM image of Al_2O_3 nanoparticles from Sohel et al. [43]

Likewise, Ataei et al. [44] used a constant heat flux heater in experiments with microchannel heat sinks to find that nanofluids can improve heat transfer by 16.97%, in good agreement with Sohel et al. While the application of nanofluids may usually increase heat transfer capabilities, their use incurs issues such as higher maintenance, agglomeration, deposition, and higher cost [21]**.** The presented studies do great work in advancing the knowledge of nanofluid performance, but similarly to the previous literature discussed in the current work, tend to focus on contrived heat sources and don’t discuss monetary impact of the nanofluids on the overall cooling system fabrication.

2.6 Literature Review Summary

Several gaps were identified in the aforementioned literature that the present work intends to address. First, whereas there is an abundance of general studies involving experimental and numerical investigations with broad boundary conditions such as uniform heat fluxes or resistors as discrete heat sources, there are fewer studies on liquid cooling heat sink design for specific electronics industry thermal problems. Second, while there are some studies which address heat sink fabrication techniques [45], there is a scarcity of studies on cost comparisons of different liquid cooling heat sink design choices. Third, although there are many studies on liquid microchannel heat sinks, pin fin heat sinks, and header designs, there are not many studies that directly compare the performance all three of these design parameters in one study for a commercially focused application. This work investigates all three of these liquid cooling heat sink design features and directly compares their thermal and hydrodynamic performance to determine the optimal choice for the specific electronics industry application. This thesis also investigates price differences for design choices such as pin size, pin density, and header angle, as well as compares prices of channel designs vs. pin designs, using a fully-fledged CNC machining prototyping company. Lastly, the current paper investigates a real-life application of computational fluid dynamics for a heat transfer problem involving a circuit board that has been manufactured and will be used in instruments at Keysight Technologies.

Chapter 3

Thermal Management Problem Description, Approach and Methods

3.1 Problem Description and Approach

The thermal management problem investigated in this thesis is illustrated in Figure 3.1. The system consists of integrated circuit (IC) chips (not shown due to non-disclosure agreements), a circuit board, two sets of thermal interface material, an aluminum EMI shield, and a liquid-cooled heat sink (metallic heat spreader and 3-D printed water block to act as the inlet and outlet of the water, as well as to seal the system), see Figure 3.1. The heat transfer path starts at the integrated circuit chips on the backside of the circuit board, goes through the circuit board, then interface material, through an aluminum shield, through more thermal interface material, through the liquid-cooled heat sink, and into the water flowing through the heat sink . Combined, the IC chips dissipate 83W of power, but act as discrete regional heat sources.

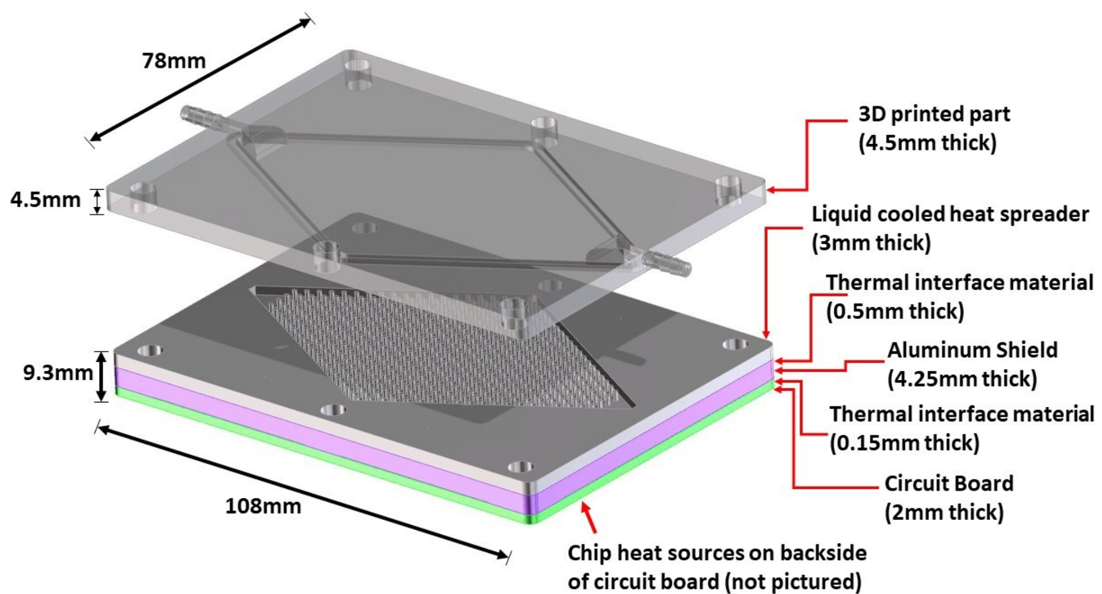

Figure 3.1: Circuit board assembly and thermal management system investigated in this thesis.

The approach used for investigating this problem was to examine the effect on performance and price of three common design features of liquid cooling heat sinks: the header design, pin fin geometry, and mini channel geometry. Specifically, the effect of diameter and spacing of the pin fin geometry and the effect of length of the mini channel geometry were investigated. Figure 3.2 depicts a top level view of a pin fin heat sink design, the PF1-15 design, see Section 3.7 for the nomenclature of the heat sink designs based on the geometry of the metallic heat spreader. Figure 3.3 illustrates a diagram showing the header angle parameter which is varied in the first simulation cases. Figure 3.4 is an illustration of the varied pin geometry (shown is the case PF1-15). Figures 3.5 and 3.6 depict the two channel designs chosen for investigation- one with long fins (MCLF) and one with short fins (MCSF).

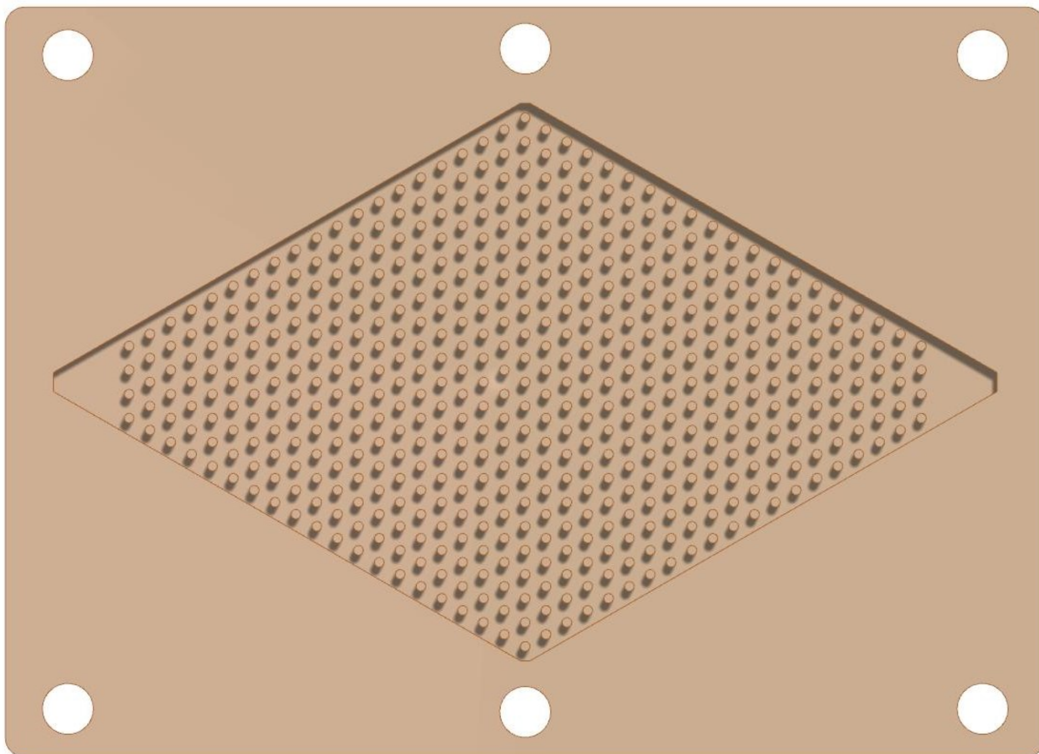

Figure 3.2: Top level view of PF1-15 design

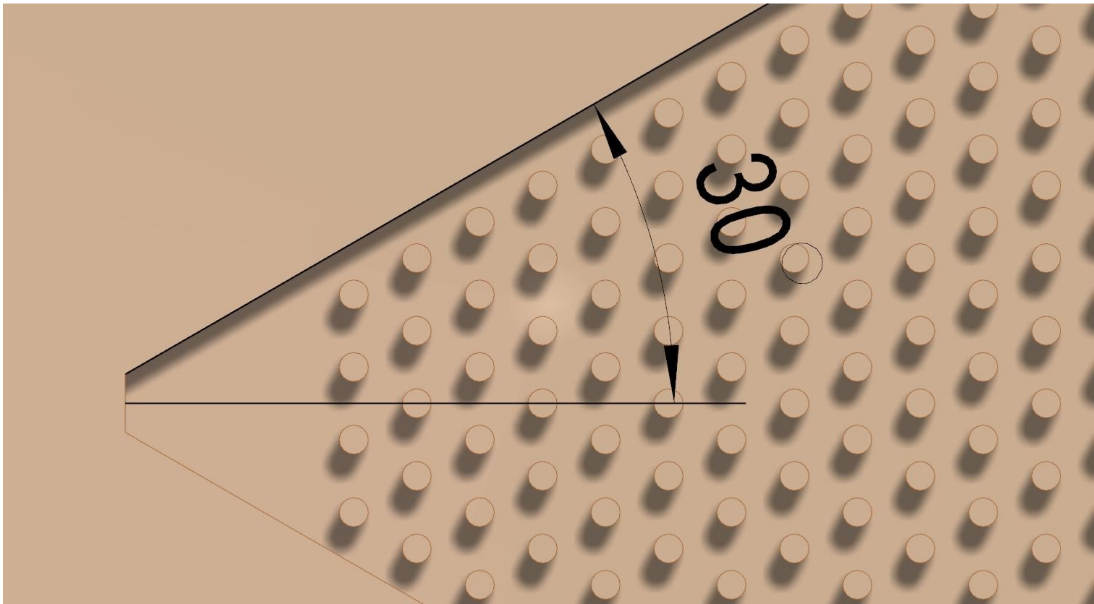

Figure 3.3: Zoomed in view showing header angle that is varied for first 4 cases (30 degree shown here).

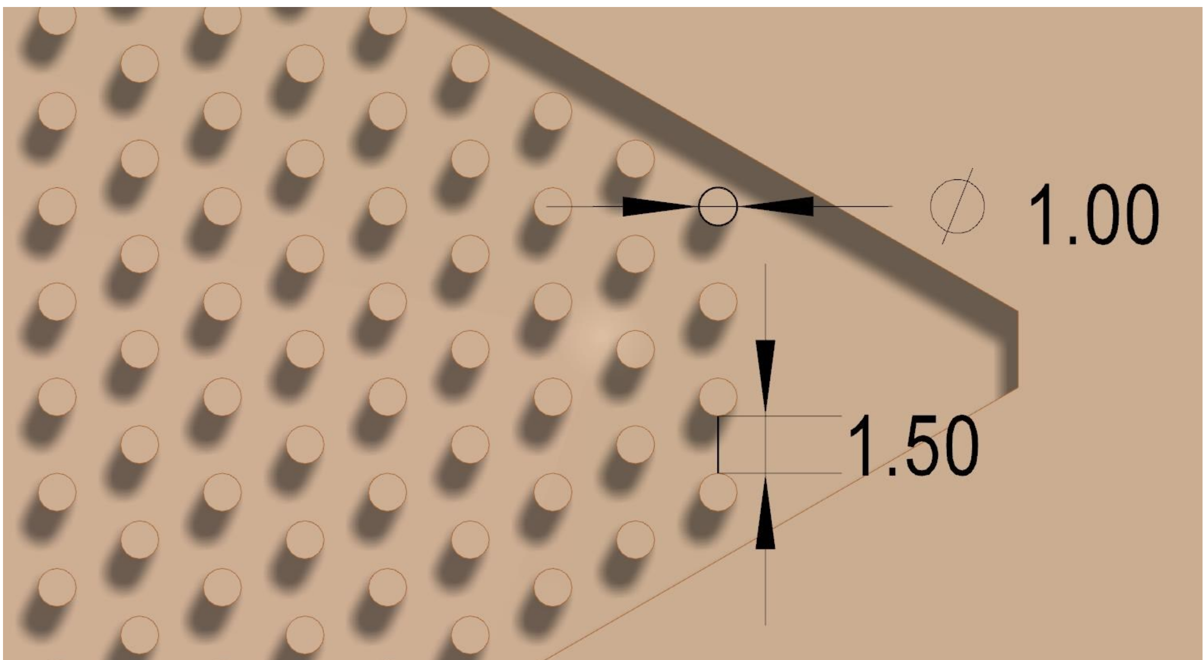

Figure 3.4: Zoomed in view of PF1-15 showing pin fin diameter and edge-to-edge spacing parameters that are varied throughout the different cases

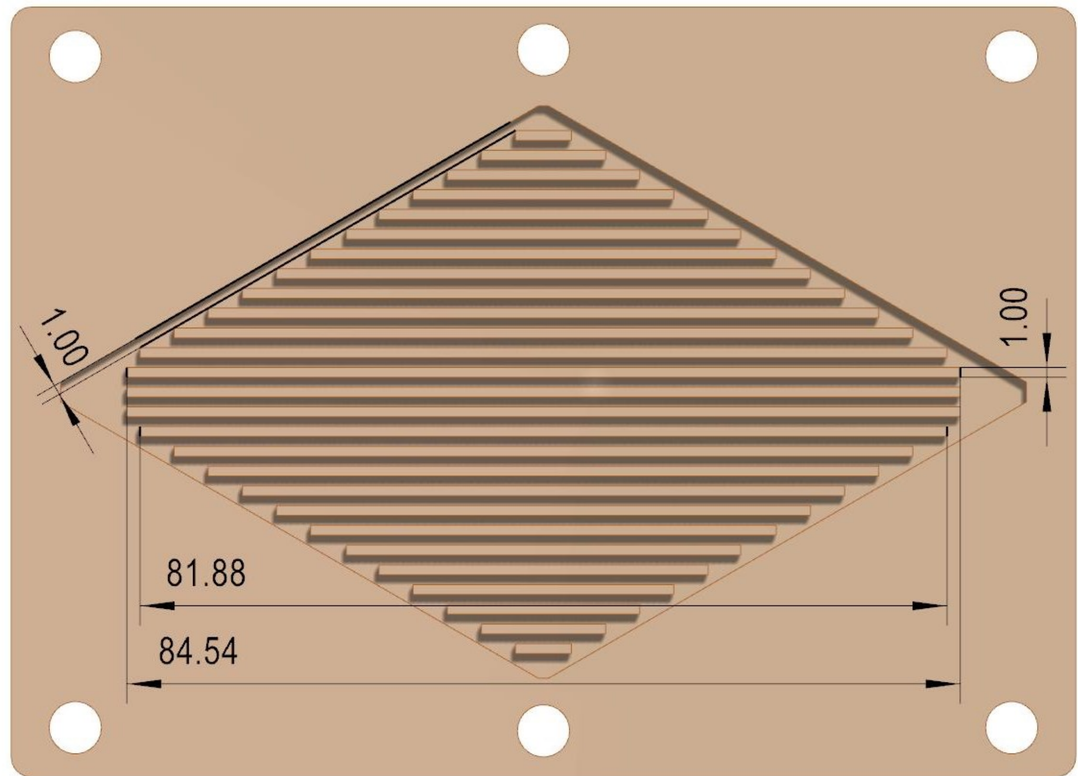

Figure 3.5: Dimensions of MCLF (mini channel long fin) heat sink.

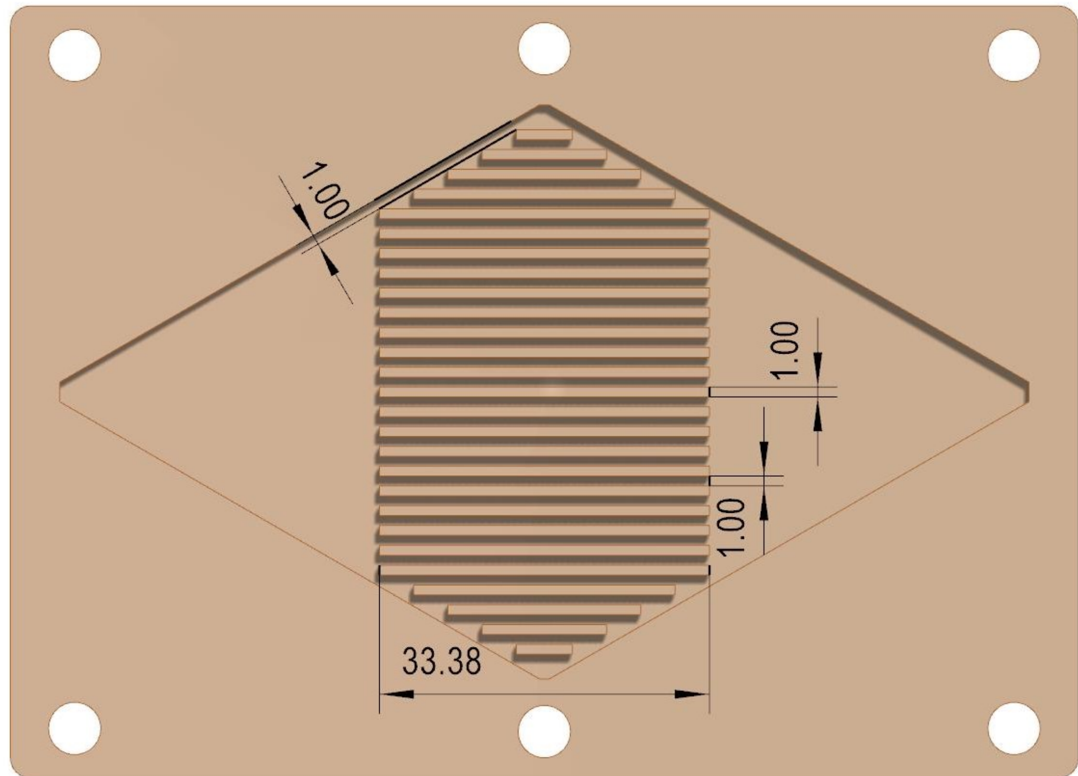

Figure 3.6: Dimensions of MCSF (mini channel short fin) heat sink.

3.2 Modeling Assumptions and Governing Equations

The hydraulic and thermal behavior of the thermal management problem depicted in Figure 3.1 was investigated using 3-D CFD simulations. Specifically, the software package Ansys Fluent 19.2 was used for the simulations. The simulations were conducted under the following assumptions:

- Steady state
- Incompressible flow
- Laminar regime when Re = 0 – 2000 (defined at the inlet)
- Turbulent flow regime when Re = 2000 – 10000 (defined at the inlet)

The hydraulic and heat transfer properties of the system can be solved by the following equations, with the momentum equations depending on whether the flow is in the laminar or turbulent regime:

- Continuity

$$\frac{\partial u}{\partial x} + \frac{\partial v}{\partial y} + \frac{\partial w}{\partial z} = 0 \tag{1}$$

- Laminar Momentum - Navier Stokes

$$\rho(u\frac{\partial u}{\partial x} + v\frac{\partial u}{\partial y} + w\frac{\partial u}{\partial z}) = -\frac{\partial p}{\partial x} + \mu(\frac{\partial^2 u}{\partial x^2} + \frac{\partial^2 u}{\partial y^2} + \frac{\partial^2 u}{\partial z^2}) \tag{2}$$

$$\rho(u\frac{\partial v}{\partial x} + v\frac{\partial v}{\partial y} + w\frac{\partial v}{\partial z}) = -\frac{\partial p}{\partial y} + \mu(\frac{\partial^2 v}{\partial x^2} + \frac{\partial^2 v}{\partial y^2} + \frac{\partial^2 v}{\partial z^2}) \tag{3}$$

$$\rho(u\frac{\partial w}{\partial x} + v\frac{\partial w}{\partial y} + w\frac{\partial w}{\partial z}) = -\frac{\partial p}{\partial z} + \mu(\frac{\partial^2 w}{\partial x^2} + \frac{\partial^2 w}{\partial y^2} + \frac{\partial^2 w}{\partial z^2}) \tag{4}$$

- Turbulent Momentum - RANS

$$\bar{u}\frac{\partial \bar{u}}{\partial x} + \bar{v}\frac{\partial \bar{u}}{\partial y} + \bar{w}\frac{\partial \bar{u}}{\partial z} = -\frac{1}{\rho}\frac{\partial \bar{P}}{\partial x} + v\left(\frac{\partial^2 \bar{u}}{\partial x^2} + \frac{\partial^2 \bar{u}}{\partial y^2} + \frac{\partial^2 \bar{u}}{\partial z^2}\right)$$
$$-\frac{\partial}{\partial x}\left(\overline{u'^2}\right) - \frac{\partial}{\partial y}\left(\overline{u'v'}\right) - \frac{\partial}{\partial z}\left(\overline{u'w'}\right) \tag{5}$$

$$\bar{u}\frac{\partial \bar{v}}{\partial x} + \bar{v}\frac{\partial \bar{v}}{\partial y} + \bar{w}\frac{\partial \bar{v}}{\partial z} = -\frac{1}{\rho}\frac{\partial \bar{P}}{\partial y} + v\left(\frac{\partial^2 \bar{v}}{\partial x^2} + \frac{\partial^2 \bar{v}}{\partial y^2} + \frac{\partial^2 \bar{v}}{\partial z^2}\right)$$
$$-\frac{\partial}{\partial x}\left(\overline{u'v'}\right) - \frac{\partial}{\partial y}\left(\overline{v'^2}\right) - \frac{\partial}{\partial z}\left(\overline{v'w'}\right) \tag{6}$$

$$\bar{u}\frac{\partial \bar{w}}{\partial x} + \bar{v}\frac{\partial \bar{w}}{\partial y} + \bar{w}\frac{\partial \bar{w}}{\partial z} = -\frac{1}{\rho}\frac{\partial \bar{P}}{\partial z} + v\left(\frac{\partial^2 \bar{w}}{\partial x^2} + \frac{\partial^2 \bar{w}}{\partial y^2} + \frac{\partial^2 \bar{w}}{\partial z^2}\right)$$
$$-\frac{\partial}{\partial x}\left(\overline{u'w'}\right) - \frac{\partial}{\partial y}\left(\overline{v'w'}\right) - \frac{\partial}{\partial z}\left(\overline{w'^2}\right) \tag{7}$$

- Energy

$$\bar{u}\frac{\partial \bar{T}}{\partial x} + \bar{v}\frac{\partial \bar{T}}{\partial y} + \bar{w}\frac{\partial \bar{T}}{\partial z} = \alpha\left(\frac{\partial^2 \bar{T}}{\partial x^2} + \frac{\partial^2 \bar{T}}{\partial y^2} + \frac{\partial^2 \bar{T}}{\partial z^2}\right) - \frac{\partial}{\partial x}\left(\overline{u'T'}\right) - \frac{\partial}{\partial y}\left(\overline{v'T'}\right) - \frac{\partial}{\partial z}\left(\overline{w'T'}\right) \tag{8}$$

ρ and μ in the equations represent the density and dynamic viscosity of water, respectively. P represents pressure and $\bar{P}$ represents time averaged pressure. The u, v and w represent the fluid velocity components in the x, y and z directions, respectively. The $\bar{u}$, $\bar{v}$, and $\bar{w}$ represent the time averaged fluid velocity components in the x, y and z directions, respectively. The u', v' and $w'$are the fluctuating fluid velocity components in the x, y and z directions, respectively. α represents the thermal diffusivity, $\bar{T}$ represents time-averaged temperature, and T' represents the fluctuations in temperature in turbulent flow.

3.3 Conduction Simulations: Addressing the Complexity of a Multiscale Heat Transfer Problem

A preliminary conduction simulation was executed to save computational time and resources, as the dimensions of different parts of the thermal management problem described in Figure 3.1 span different length scales, from a few micrometers to several millimeters. If done in full, plenty of computational power would be required for accurately describing the boundary layer around several millimeter scale features, in addition to properly discretizing the temperature profiles in micrometer scale layer of materials. Thus, the heat transfer problem was divided in two, a conduction and a convection problem. The conduction simulation results were used as boundary conditions for the convection liquid cooling simulations. In the preliminary conduction simulation, Ansys Fluent was used to simulate the conduction of the Keysight circuit board by modeling each chip as a series of layers with a specified heat flux. Due to the sensitive nature of

this circuit board as intellectual property, the details of the chip layers and chip configuration cannot be disclosed. In this set of conduction simulations, varying convective coefficients were applied at the top face of the circuit board assembly until acceptable backside chip temperatures were achieved. Eventually, a convective coefficient of 2000 W/m^2-ºC was found to provide sufficient cooling. This coefficient will be matched by the total thermal conductance parameter in the convection liquid cooling sims to ensure that the liquid cooling heat sink is cooling the system adequately. Then, the temperature rise calculated from the convection simulations at different flow rates will match the power dissipated in the conduction problem, i.e., 83 W. With the coefficient of 2000 W/m^2-ºC, the Ansys simulation yielded results in the form of a temperature contour across the top face of the circuit board assembly illustrated in Figure 3.7.

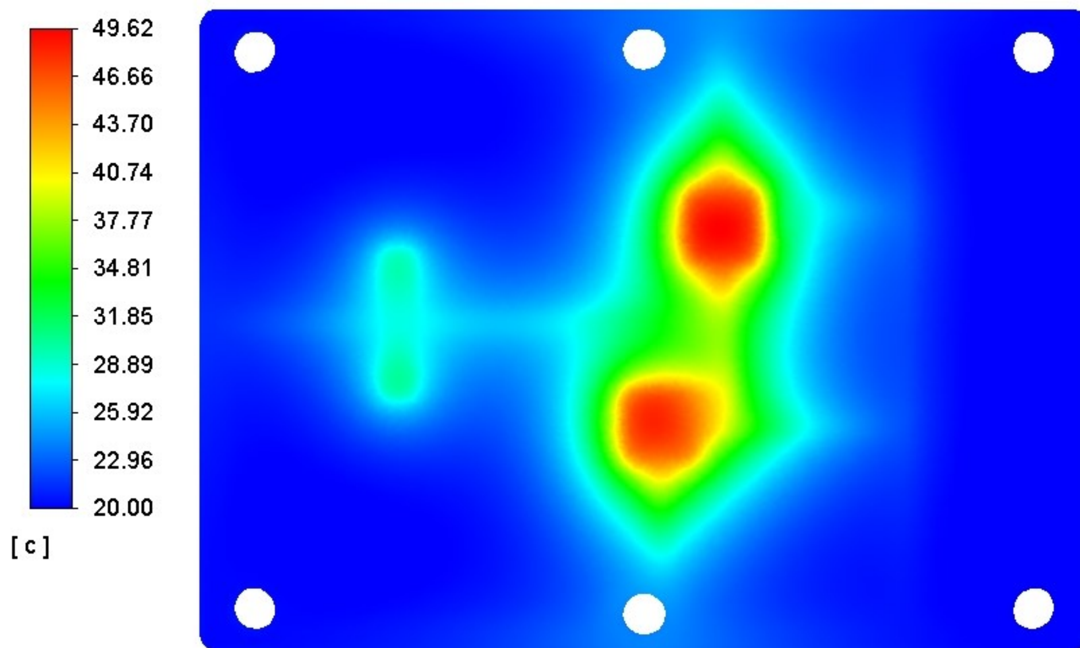

Figure 3.7: Temperature contour results from the conduction simulations.

3.4 Boundary Conditions, Operating Conditions, and Properties

The commercial computational fluid dynamics software package Ansys Fluent 19.1 was used to solve the governing equations (1-8) for velocity, pressure, and temperature. Ansys Fluent uses the Finite Volume Method for solving the differential equations. The following parameters were used for the Ansys Fluent solver: energy equation on, standard k-epsilon turbulence model, SIMPLE scheme, and all residuals below 1E-06. These parameters were chosen because they are consistent with many previous studies of this nature in the literature. In addition to these parameters, the inlet pressure and outlet temperature were tracked for asymptotic convergence across iterations as well. The material properties used in the simulations for this thesis are shown in Table 1.

Table 1: Material Properties

Symbol	Value	Description	Units
c_p	4182	Specific heat of water	(J/kg°C)
ρ	997	Density of water	kg/m^3
Area	0.0083	Area of top of circuit board assembly	m^2
$\dot{m}$	Varies from 0.001 to 0.01 with spacings of 0.001	Mass flow rate	(kg/s)

3.5 Performance Evaluation Metrics

Table 2 shows the metrics used to evaluate the performance of the heat sinks. ΔP, $T_{surfavg}$, and T_{out} are raw data values obtained from the CFD simulations. Q, R, G, PP, PPTC and PPTC/$ are values derived from the raw data. The primary parameters used for evaluation are the total thermal conductance (G), pumping power (PP), and price. G is a measure of how well the heat sink transfers heat to the fluid, and thus how well it will cool the system. Recall that in order to cool the Keysight Technologies circuit board, a G value of 2000 W/m^2-°C is required. PP is the

amount of power required for the fluid to be pumped through the heat sink. Price is the manufacturing price of the heat sink in US dollars, as quoted with Protolabs' online auto-quote tool. The PPTC is a parameter that considers the pumping power and the total thermal conductance. The PPTC/$ is the PPTC divided by the price of manufacture, thus wrapping thermal performance, hydraulic performance, and manufacturing price into one metric for effective comparison. The PPTC and PPTC/$ metrics are described in detail in chapter 4.5 in this thesis.

Table 2: Performance Evaluation Metrics

Symbol	**Value**	**Description**	**Units**
ΔP	N/A	Inlet-outlet pressure drop	(Pa)
$T_{surfavg}$	N/A	Surface average temperature	(ºC)
T_{in}	N/A	Inlet fluid temperature	(ºC)
T_{out}	N/A	Outlet fluid temperature	(ºC)
q	$\dot{m}*cp(T_{out} - T_{in})/Area$	Heat flux	(W)
R	$(T_{surfavg} - T_{in})/q$	Total thermal resistance of heat sink	(ºC-m^2/W)
G	1/R	Total thermal conductance of heat sink	(W/ºC-m^2)
PP	$\dot{m}*\Delta P/\rho$	Pumping Power	(W)
Price	N/A	Manufacturing price of heat sink	(US Dollars)
PPTC	N/A	Pumping power thermal conductance parameter	(W/ºC-m^2)
PPTC/$	PPTC/Price	Pumping power thermal conductance parameter per US dollar	(W/ºC-m^2)/$

3.6 Mesh Independence

To ensure that the simulation solution is not dependent on the resolution of the mesh, a mesh independence study must be carried out. A mesh independence study involves running successive simulations with increasing mesh elements while comparing certain parameters of each simulation. Once the parameters in two successive simulations are sufficiently close in value, mesh independence has been achieved. In this thesis, the two parameters compared were

pressure drop and outlet temperature. Between 11.04 million and 12.64 million elements, an acceptable mesh independence was achieved with a 3% and 0.005% difference in pressure drop and outlet temp, respectively. Thus, for the remainder of the simulations run for this thesis, a mesh resolution of at least 11.04 million elements was used. Table 2 summarizes the results of the mesh independence study. Figure 3.8 shows the 12.6 million element mesh.

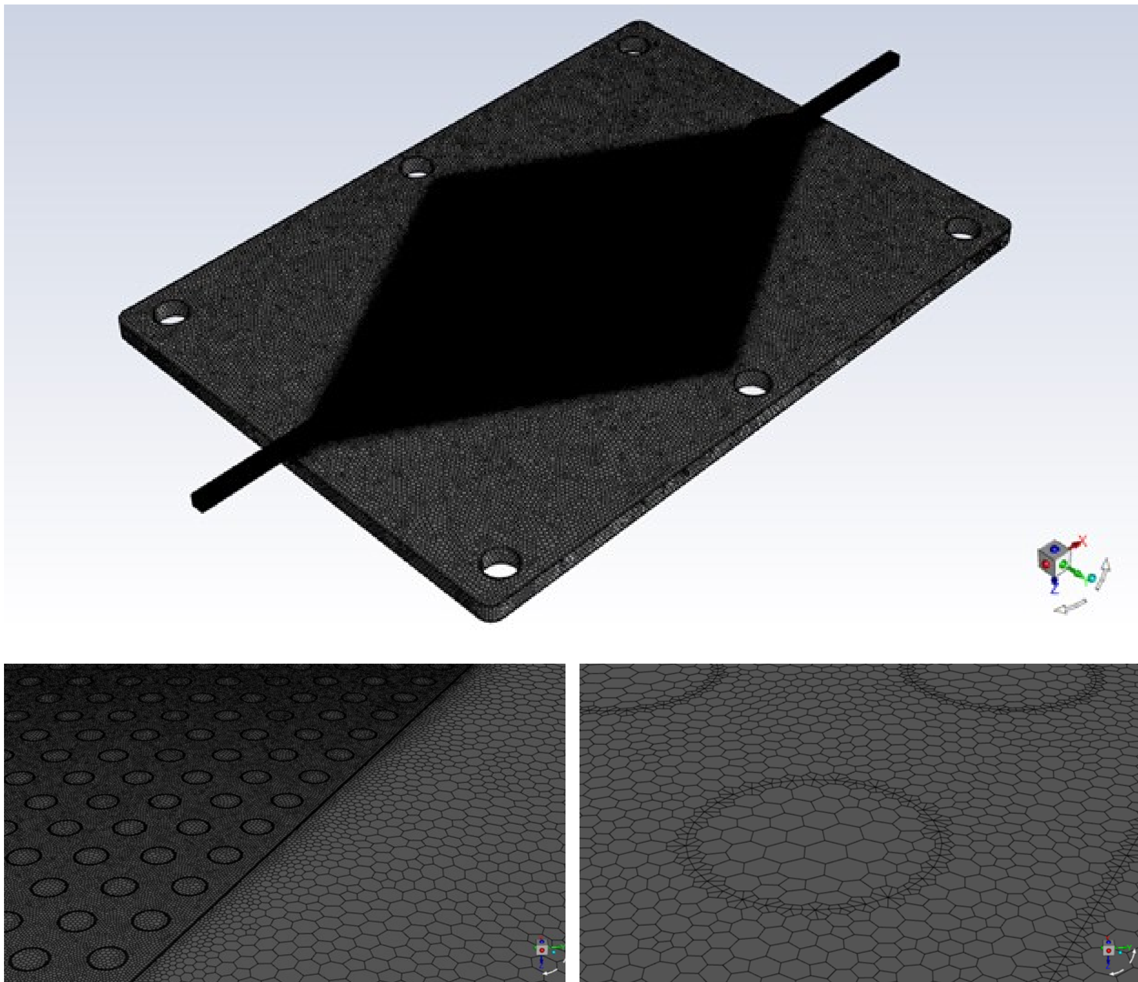

Figure 3.8: 12.6 million element mesh, successively zoomed in on pin fins.

Table 3: Mesh Independence Study Results

Number of Mesh Elements	Pressure Drop (Pa)	Outlet Temp. (ºC)
2,095,572	11,936.16	26.84
4,391,143	12,814.64	26.96
7,479,280	14,187.72	27.05

11,044,411	15,283.66	27.09
12,637,621	15,793.04	27.09

3.7 Convection Simulation Procedure

In the convection phase of the simulations, fluid flow through different types of liquid-cooled heat sink designs were modeled. Note that all phase 2 simulations were run at ten flow rates evenly spaced between 0.001 and 0.01 kg/s. These simulations used the temperature distribution result of Section 3.3 as a boundary condition on the bottom of the heat sinks, and then verified that a conductance of 2000 W/m^{2}C was achieved when the temperatures rise in the water was equivalent to dissipating 83 W from the conduction simulation. First, four simulations were run with the only variable between the four being the header angle. The header angle was chosen as a parameter to investigate because studies and literature have shown that the header angle dramatically effects flow distribution, and thus heat transfer performance, of liquid-cooled heat sinks. These four cases all had 1mm diameter, 1mm edge-to-edge spaced pin fins. Figure 3.2 shows the header angles which were varied at 30, 50, 70, and 90 degrees in these first four cases. Next, the effect of spacing between the fins was investigated. After, four cases with pin fins of 0.5mm diameter were run with varying edge-to-edge spacing of 0.5mm, 1mm, 1.5mm, and 2mm. The next three simulations were run with 1.5mm diameter pin fins with varying edge-to-edge spacing of 1mm, 1.5mm, and 2mm. See Table 3.2 for the heat sink geometry parameters used in the simulations.

Consecutively four cases with plate fins instead of pin fins for comparison were run for comparison. The plates will vary in plate spacing and plate length. After these four plate fin cases, a series of air-cooled simulations may be run in order to compare the physical size/volume requirements of air cooled heat sinks versus liquid cooled heat sinks. Lastly, if time permits,

several simulations may be run using the best performing liquid cooling heat sink geometries with aluminum material instead of copper to compare the effect of changing the material, and whether the cheaper material can still be adequate to cool the system while also dropping monetary costs.

Table 4: Pin fin heat sink geometry parameters

Case Label	Pin Diameter (mm)	Edge-to-Edge Spacing (mm)	Header Angle (degrees)
PF30/PF1-1	1	1	30
PF50	1	1	50
PF70	1	1	70
PF90	1	1	90
PF1-15	1	1.5	30
PF1-2	1	2	30
PF05-1	0.5	1	30
PF05-15	0.5	1.5	30
PF05-2	0.5	2	30
PF15-1	1.5	1	30
PF15-15	1.5	1.5	30
PF15-2	1.5	2	30

Table 5: Mini channel heat sink geometry parameters

Case Label	Fin Length	Edge-to-Edge Spacing (mm)	Header Angle (degrees)
MCLF	Long	1	30
MCSF	Short	1	30

Table 6: Select cases using aluminum

Aluminum Case Label	Original Case Label
PF1-1-AL	PF1-1
MCSF-AL	MCSF

Chapter 4

Simulation Results and Discussion

4.1 Header Design

In this section, the results from the varying header angle heat sink simulations will be presented and discussed. Figure 4.1 shows the total thermal conductance G versus mass flow rate $\dot{m}$. This figure shows an increasing total thermal conductance with increasing mass flow rate, which is to be expected based on fluid dynamics and heat transfer fundamentals. It can also be seen from this figure that, across all mass flow rates, the 30 degree header angle design (PF30) has a higher total thermal conductance than the other three header angles. This aligns with previous research , including the study by Radwan et al. [46], showing that a tighter header angle allows for better flow distribution, less wasted heat sink area, and thus better heat transfer. Recall from chapter 3 that as a design criterion, the heat sink must have a total thermal conductance of at least 2000 W/m^2-ºC. The PF30 heat sink achieves this at fairly low flow rates, starting at approximately 0.003kg/s. The PF50 design achieves this at 0.004kg/s, and the PF70 and PF90 both achieve this at approximately 0.005kg/s. This indicates that all designs satisfy the cooling needs of the Keysight circuit board at these threshold flow rates. Higher flow rates will theoretically cool the circuit board more than required.

Figure 4.2 shows the pressure drop versus mass flow rate for the four header angle designs. The figure shows an increasing pressure drop with increasing mass flow rate across all designs, which is expected. The figure also shows a trend with pressure drop at any given flow rate, with pressure drop going from lowest to highest in the order of PF90, PF70, PF50, and

PF30. At lower flow rates this pressure drop difference between the header designs is negligible while at higher flow rates it becomes more significant.

Figure 4.3 shows the total thermal conductance versus pumping power for the four different header designs as a more comprehensive evaluation of the overall performance of the heat sinks, including pressure losses and heat transfer metrics. Figure 4.3 is an important figure of merit, as it directly compares the hydraulic cost of operating a liquid-cooled heat sink with its thermal performance. By illustrating thermal conductance as a function of pumping power, it is possible to draw general conclusions on the overall performance of the heat sinks considered herein, given the inconclusive tradeoff between cooling and pressure losses, see Figures 4.1 and 4.2. Hence, it is desirable to obtain the largest cooling capabilities at the lowest pumping power requirement. Figure 4.3 shows a general trend of overall performance over a range of pumping powers, from lowest to highest, of PF90, PF70, PF50, and PF30. Nonetheless, it also shows that PF90 and PF70 have similar overall performance, indicating that the minute cooling and pressure losses differences between these two designs, create an almost zero net gain in overall performance. Lastly, Figure 4.4 shows the prices in US dollars for the four different metallic plates compatible with the different header designs. The prices in this thesis were quoted from Protolabs' online auto-quote tool. The material used for quoting was copper in all cases unless otherwise stated. In figure 4.4, a trend is shown in which increasing the header angle increases the price of the heat sink, as the wider the angle the more pin fins must be machined on the plate. The outcome of the 30 degree header angle design having the best overall performance, as well as price compared to the other designs, drove the decision to proceed with the 30 degree header angle for all consecutive optimization simulations of this thesis.

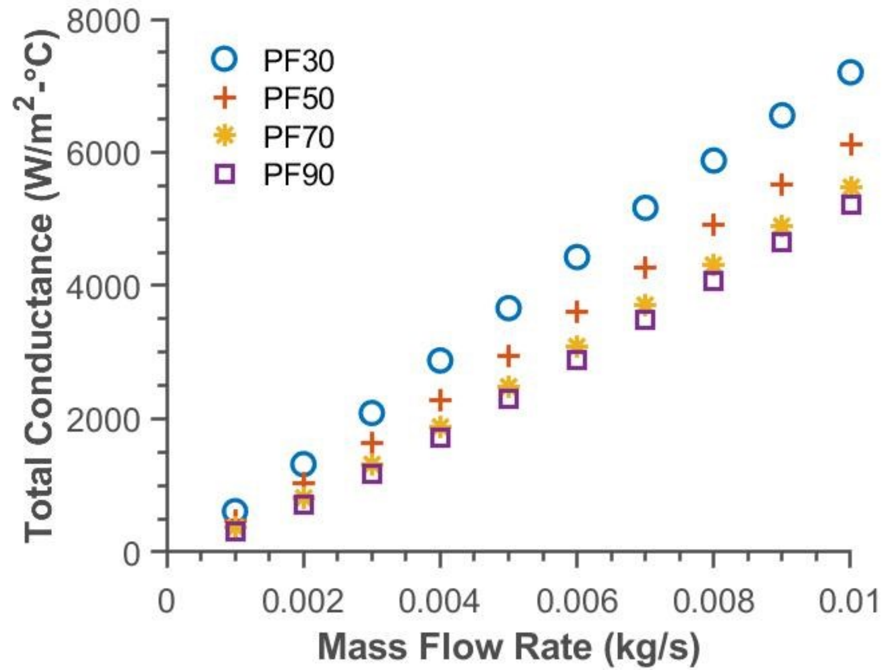

Figure 4.1: Total thermal conductance vs. mass flow rate for the 30 degree, 50 degree, 70 degree and 90 degree angle header designs.

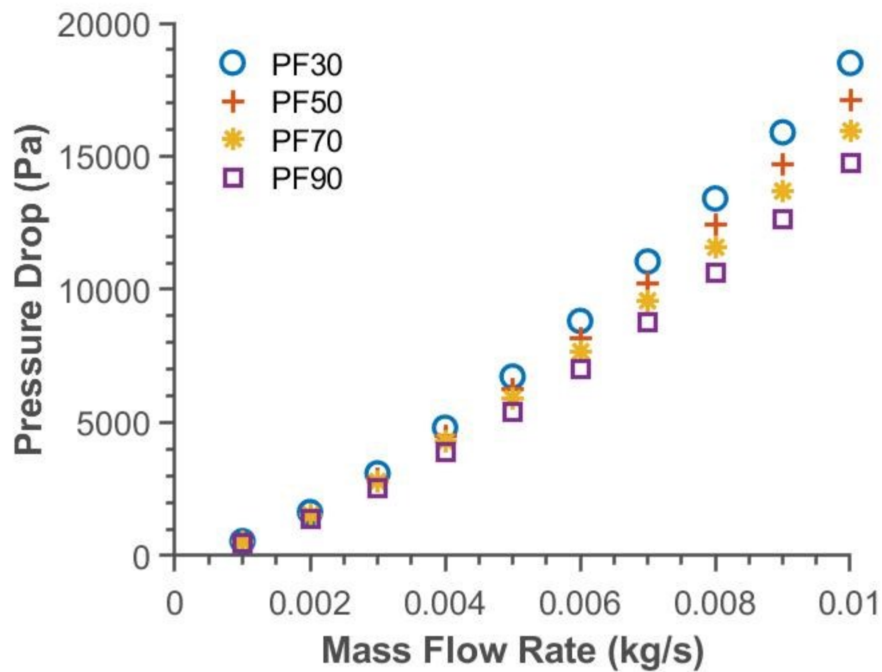

Figure 4.2: Pressure drop vs. mass flow rate for the 30 degree, 50 degree, 70 degree and 90 degree angle header designs.

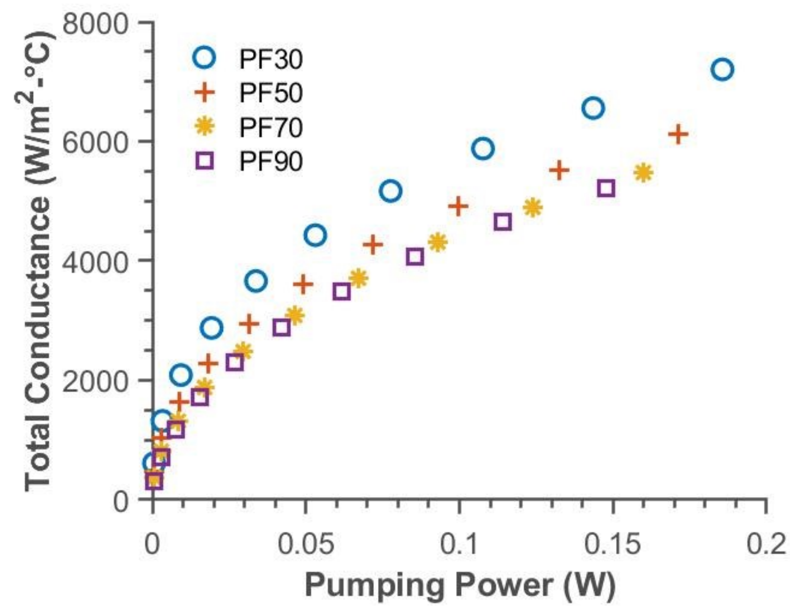

Figure 4.3: Total thermal conductance vs. pumping power for the 30 degree, 50 degree, 70 degree and 90 degree angle header designs.

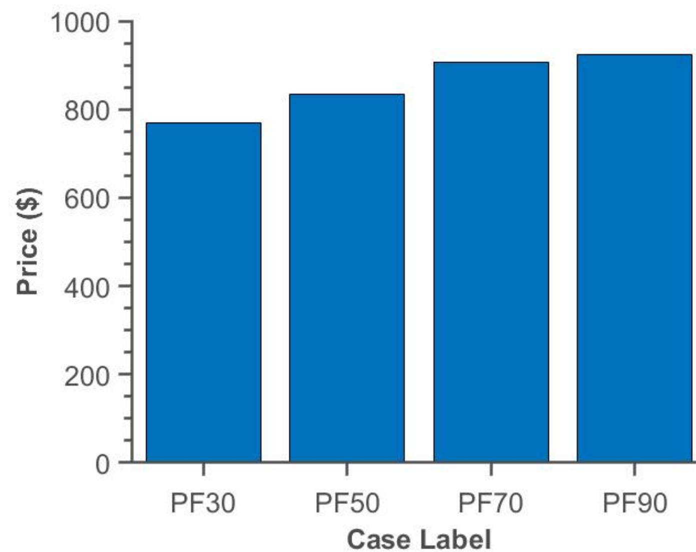

Figure 4.4: Prices for the 30 degree, 50 degree, 70 degree and 90 degree angle metallic plates compatible with the header designs.

4.2 Pin Fin Design

In this section, the results from the pin fin simulations will be presented and discussed. Recall from Table 3 and Figure 3.6 that both the pin diameter and pin edge-to-edge spacing was varied. First, the simulation results comparing varying pin spacing and holding diameter constant will be presented and discussed in sections 4.2.1 through section 4.2.3. Then the simulation results comparing varying pin diameter and holding edge-to-edge spacing will be presented in sections 4.2.4-4.2.6.

4.2.1 Pin Fin Varying Spacing: 0.5mm Diameter

In this section, results from varying the pin fin spacing and holding their diameter at 0.5mm will be presented and discussed.

Figure 4.5 shows the total thermal conductance versus mass flow rate for the pin fin heat sinks with 0.5mm diameter and 1mm, 1.5mm, and 2mm edge-to-edge spacing. At flow rates below 0.008kg/s, the 1mm spacing has the highest total thermal conductance (G) values out of the four cases and the 0.5mm spacing design has the lowest. At flow rates below 0.004kg/s, the G values of all three cases stay close. Starting at 0.004kg/s flow rate, and continuing at all higher flow rates, the trend becomes that smaller spacing yields higher G values. One reason for this is that smaller spacing allows for more fins in the design, which translates to more surface area for heat transfer between the heat sink and the fluid. Another contributor to this behavior is the increased heat transfer that comes with enhanced mixing in the wake of pin fin rows due to higher flow rates and the transition from the laminar flow regime into the turbulent flow regime. Another important result to note from this figure is the three heat sinks' achievement of a G value at least 2000 W/m^2-ºC. All of the cases achieve this by flow rate of 0.003kg/s, and the PF05-15 achieves

it slightly sooner than the others. Beyond 0.003kg/s, however, all heat sinks have achieved this G value and thus it is expected that they can adequately cool the Keysight Technologies circuit board described in chapter 3 at higher flow rates as well.

Figure 4.6 shows the pressure drop versus mass flow rate for the pin fin heat sinks with 0.5mm diameter and 1mm, 1.5mm, and 2mm edge-to-edge spacing. The trend across all flow rates is, from highest to lowest pressure drop, 1mm, 1.5mm and 2mm spacing designs. This behavior is expected and easily explained by the fact that fluid will have to be “pushed” harder through smaller spaces with the smaller edge-to-edge spacing, and thus will have higher pressure drops at smaller spacings. This figure also shows that the pressure drop increases at a quicker rate as flow rate increases.

Figure 4.7 shows the total thermal conductance versus pumping power for the pin fin heat sinks with 0.5mm diameter and 1mm, 1.5mm, and 2mm edge-to-edge spacing. This figure illustrates that, while the PF05-1 design has higher thermal conductance, this improved heat transfer performance comes at a steep pumping power cost.

Figure 4.8 compares the unit prices for the metallic plates with 0.5mm diameter and 0.5mm, 1mm, 1.5mm, and 2mm spacings manufactured in copper. As the spacing between the pin fins grows, the price decreases. This is most likely because spreading out the fins allow for fewer small features to be machined into the metal, and larger diameter tool bits to be used which will complete the machining faster, thus decreasing the manufacturing cost.

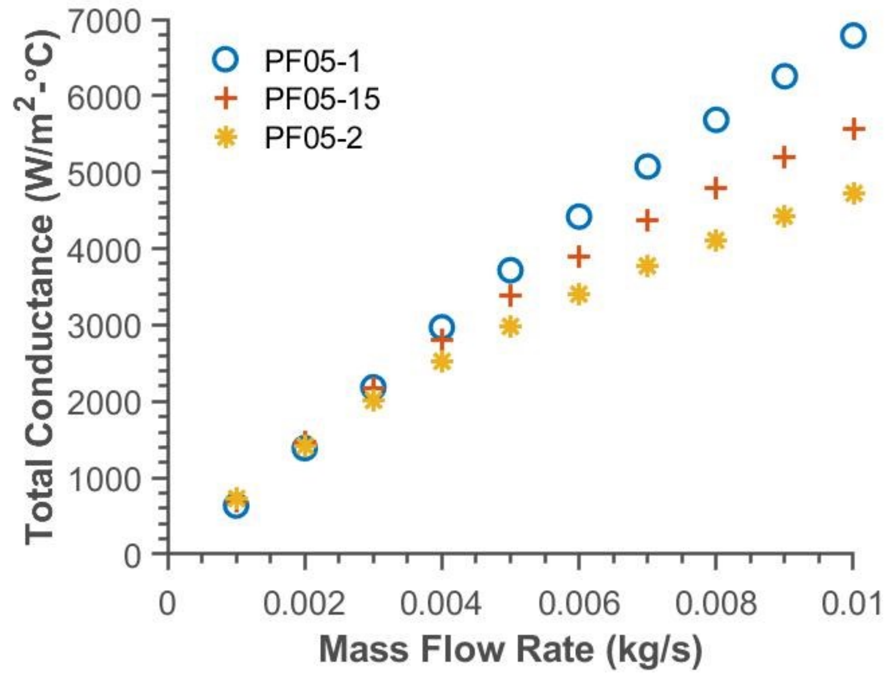

Figure 4.5: Total thermal conductance vs. mass flow rate for pin fin heat sink with 0.5mm diameter and 1mm, 1.5mm, and 2mm spacing.

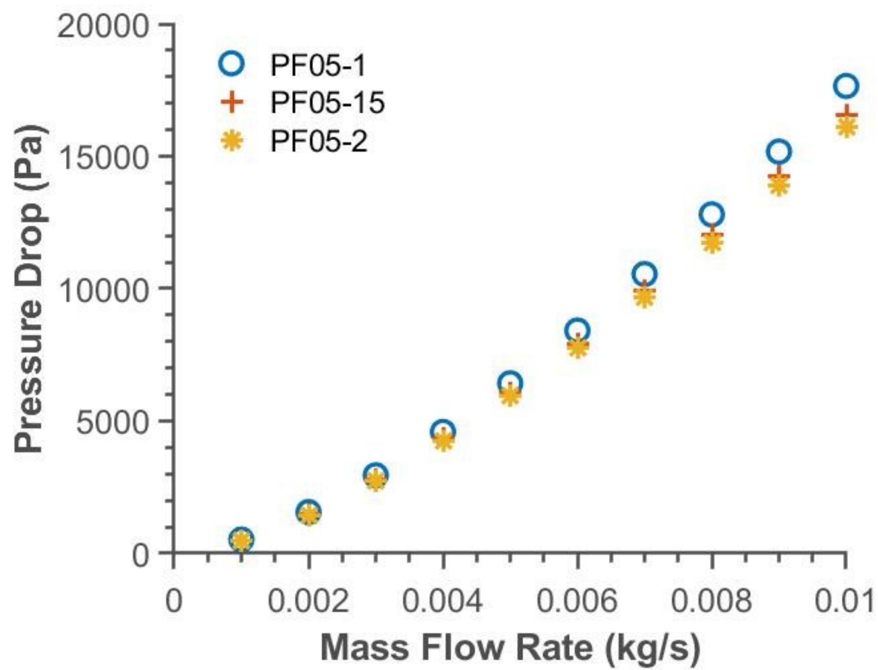

Figure 4.6: Pressure drop vs. mass flow rate for pin fin heat sink with 0.5mm diameter and 1mm, 1.5mm, and 2mm spacing.

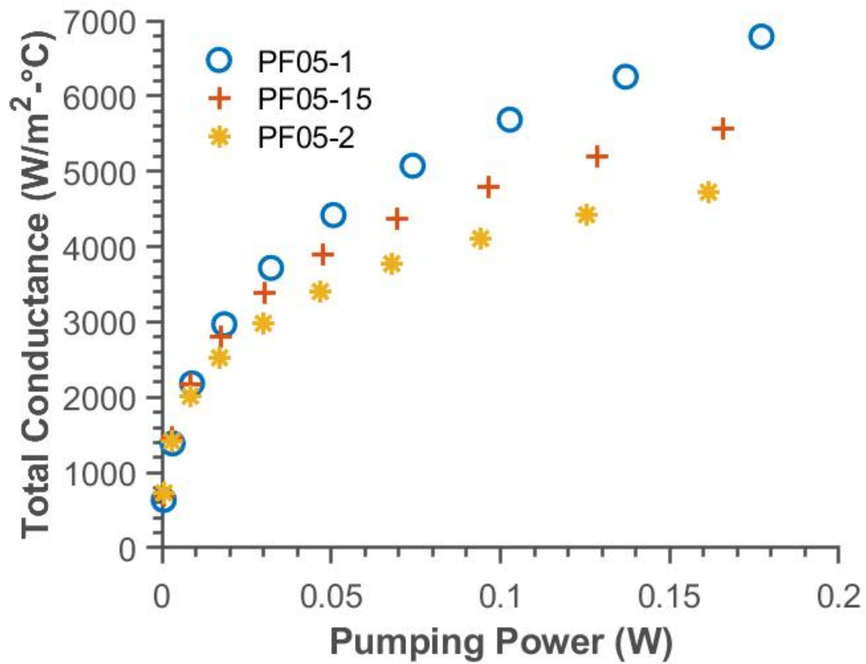

Figure 4.7: Total thermal conductance vs. pumping power for pin fin heat sink with 0.5mm diameter and 1mm, 1.5mm, and 2mm spacing.

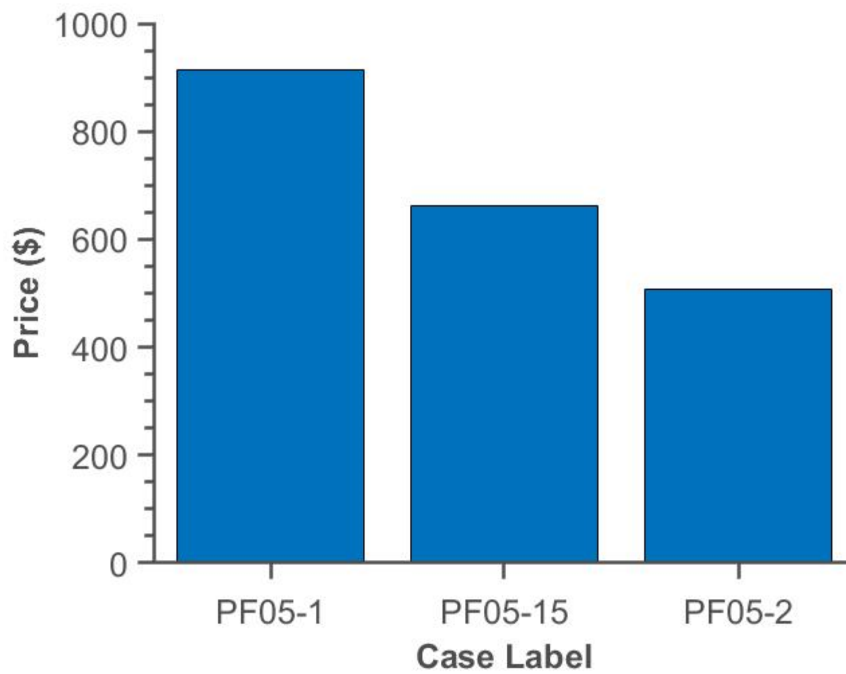

Figure 4.8: Price for pin fin heat sink with 0.5mm diameter and 0.5mm, 1mm, 1.5mm, and 2mm spacing

4.2.2 Pin Fin Varying Spacing: 1mm Diameter

Figure 4.9 depicts the total thermal conductance vs. mass flow rate for the pin fin heat sinks with 1mm diameter and 1mm, 1.5mm, and 2mm spacing. At flow rates below 0.003kg/s, the G calculations are largely undistinguishable among the different heat sinks; while at flow rates larger than 0.003kg/s, the more closely spaced fins surpass the farther spaced designs in G value. This can be explained in a similar manner as in section 4.2.1 due to two reasons: 1) the observation of higher velocities across the cross section formed between fins in closely spaced fin designs increases the local heat transfer coefficients and 2) the effective heat transfer area enhancement (i.e., more fins per unit area) in designs with closely spaced fines. This figure also shows that all three designs have a G value of 2000 W/m^2-ºC starting at a flow rate of 0.003kg/s, meaning that at this flow rate and higher, all designs can adequately cool the Keysight Technologies circuit board.

Figure 4.10 shows pressure drop vs. mass flow rate for the pin fin heat sinks with 1mm diameter and 1mm, 1.5mm, and 2mm spacing. Across all flow rates, the pressure drop is the lowest with PF1-2 and increases with decreasing fin spacing. This is expected and explained in previous sections (i.e., lower local hydraulic resistance). Of note here is that at flow rates above 0.002kg/s, the pressure drop of PF1-1 begins to sharply diverge from the other two cases, while the pressure drops of the PF1-15 and PF1-2 cases remains similar in magnitude across the range of flow rates. This divergence of PF1-1 pressure drop increases as flow rate increases.

Figure 4.11 shows total thermal conductance vs. pumping power for the pin fin heat sinks with 1mm diameter and 1mm, 1.5mm, and 2mm spacing. This figure illustrates the pumping power cost for the improved thermal conductivity, particularly for case PF1-1. For example,

between flow rates of 0.009kg/s and 0.01kg/s, PF1-1 gains about 500 W/m^2-ºC, but also increases it's required pumping power by about 0.04W. This is in contrast to the flow rate step below it between 0.008kg/s and 0.009kg/s, where it gains 500 W/m^2-ºC but only increases its required power by 0.03W. Thus, diminishing returns can be seen as flow rates become higher. From the technical point of view, PF1-1 and PF1-15 have a similar overall performance and outperform PF1-2 in the range of operating conditions considered here; thus, the manufacturing cost will allow to determine the most viable option.

Figure 4.12 shows the prices for the pin fin heat sinks with 1mm diameter and 1mm, 1.5mm, and 2mm spacing manufactured in copper. From lowest price to highest price, the heat sink designs are ordered PF1-2, PF1-1, and PF1-15. PF1-2 being the cheapest design makes sense because this design would be machined using the largest tool bit, requiring the least amount of machine time, and cost the least.

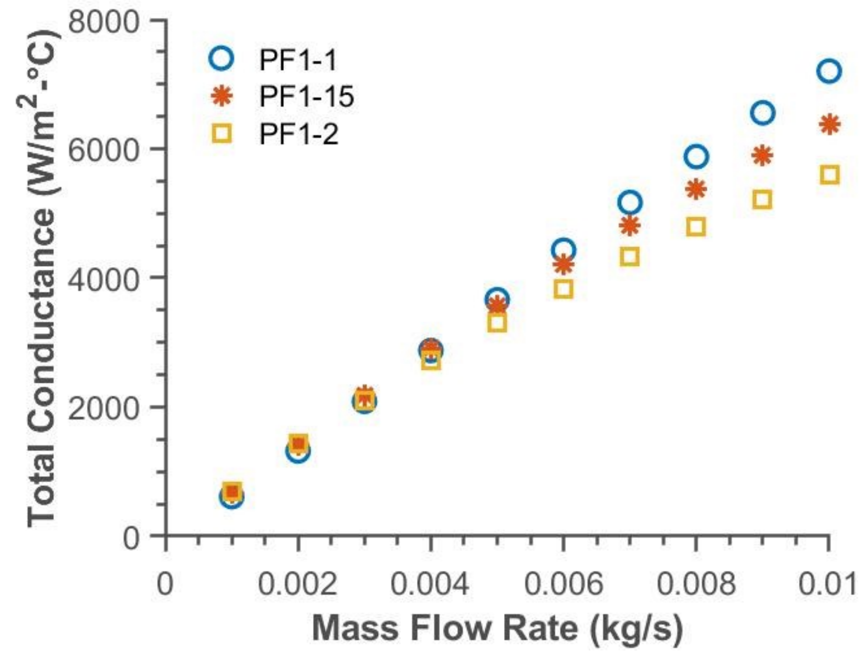

Figure 4.9: Total thermal conductance vs. mass flow rate for pin fin heat sink with 1mm diameter and 1mm, 1.5mm, and 2mm spacing.

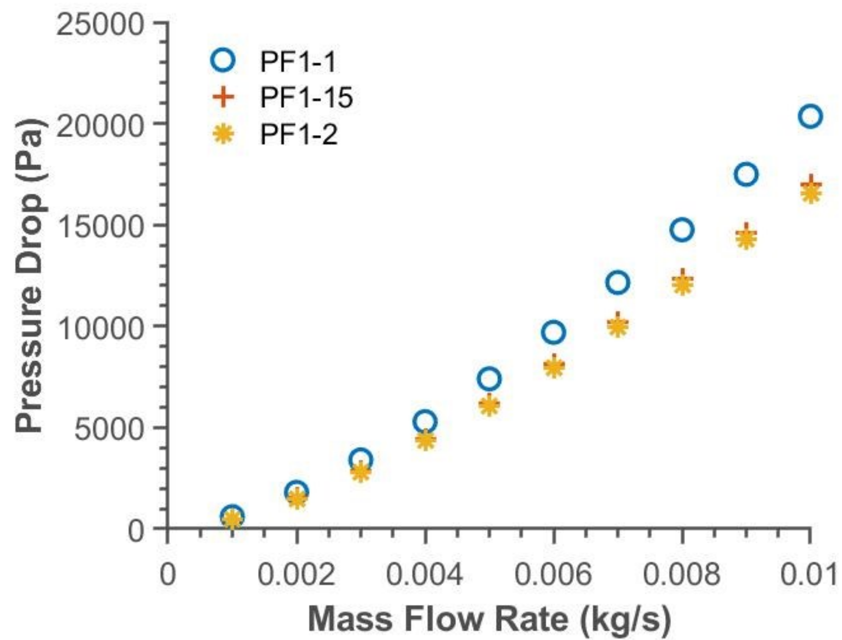

Figure 4.10: Pressure drop vs. mass flow rate for pin fin heat sink with 1mm diameter and 1mm, 1.5mm, and 2mm spacing.

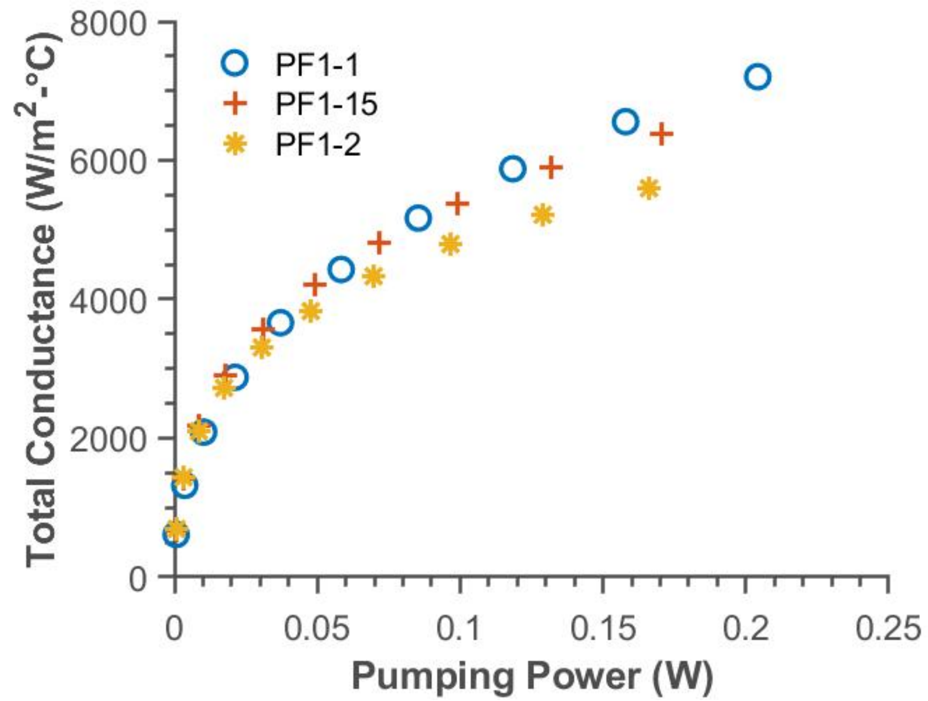

Figure 4.11: Total thermal conductance vs. pumping power for pin fin heat sink with 1mm diameter and 1mm, 1.5mm, and 2mm spacing.

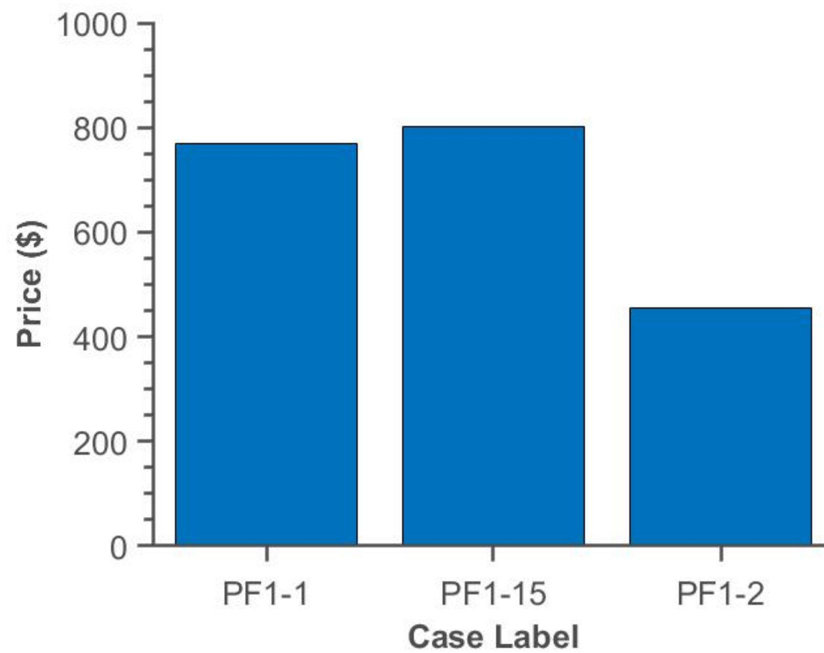

Figure 4.12: Prices for pin fin heat sink with 1mm diameter and 1mm, 1.5mm, and 2mm spacing.

4.2.3 Pin Fin Varying Spacing: 1.5mm Diameter

Figure 4.13 shows the total thermal conductance vs. mass flow rate for the pin fin heat sink with 1.5mm diameter and 1mm, 1.5mm, and 2mm spacing. At flow rates below 0.004kg/s, the figure shows a rather similar G for all the heat sink designs. After 0.004kg/s flow rate, the more closely spaced fin designs have larger G values than the farther spaced fin designs. Like previous sections, this can be explained by with the transition to turbulent flow due to higher flow velocities in between fins, and the enhanced surface area due to a larger area density of fins. Also of note is that starting at a flow rate of 0.003kg/s, all cases achieve a G value of 2000 W/m^2-ºC. This indicates that at this flow rate and higher, all cases will cool the Keysight Technologies circuit board adequately.

Figure 4.14 shows the pressure drop vs. mass flow rate for the pin fin heat sink with 1.5mm diameter and 1mm, 1.5mm, and 2mm spacing. This figure shows the familiar trends of increasing pressure drop with increasing mass flow rate, as well as increasing pressure drop with decreasing fin spacing. This is because of the inverse relationship between pressure losses and flow constriction size. Similar to the previous section, the pressure of the closest spaced fin design diverges sharply at a certain flow rate (0.005kg/s here), while the other two farther spaced fin designs stay relatively close in magnitude.

Figure 4.15 shows the total thermal conductance vs. pumping power for pin fin heat sink with 1.5mm diameter and 1mm, 1.5mm, and 2mm spacing. The figure displays the pumping power cost of increased total conductance for the different designs. Once again, higher flow rates allow for decreasingly higher thermal conductivities with increasing pumping power, meaning diminishing returns can be observed for all designs. However, these diminishing returns are much more dramatic for the farthest spaced pin fin design PF15-2. If we consider the minimum

threshold value of 2000 W/m^2-ºC, which satisfies the cooling needs of the Keysight Technologies circuit board, any of the three heat sink designs could be used without any clear technical advantage of one over the other, as they have similar pumping power requirements. Above this threshold limit, clearly the PF15-1 design offers a more robust cooling option, but not as significant as the previous cases considered. Therefore, a determining parameter for the selection of a heat sink out of this set will be financial.

Figure 4.16 shows prices for the pin fin heat sink with 1.5mm diameter and 1mm, 1.5mm, and 2mm spacing. The prices go in order from lowest to highest of P15-2, PF15-1, and PF15-15.

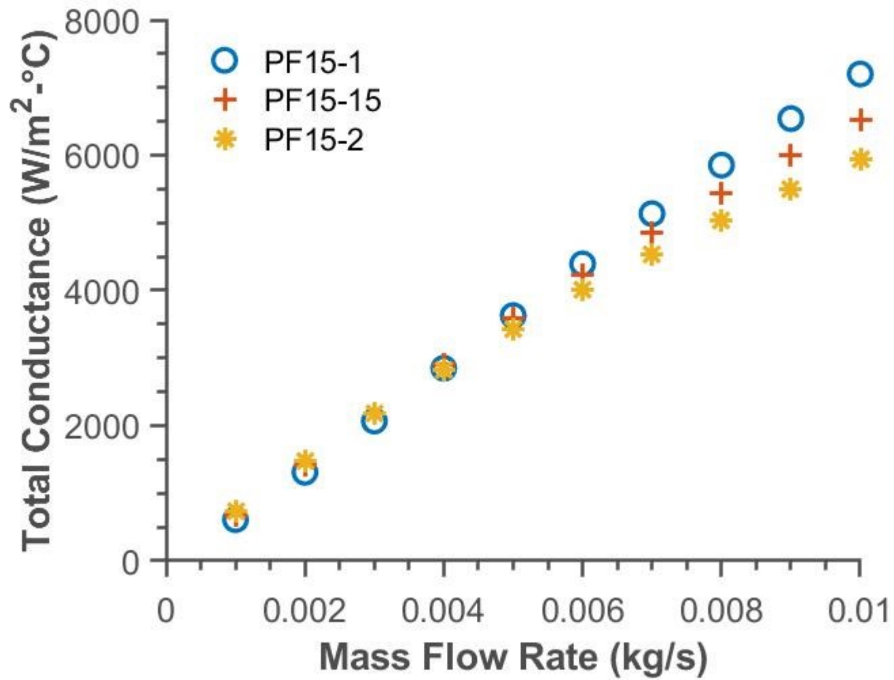

Figure 4.13: Total thermal conductance vs. mass flow rate for pin fin heat sink with 1.5mm diameter and 1mm, 1.5mm, and 2mm spacing.

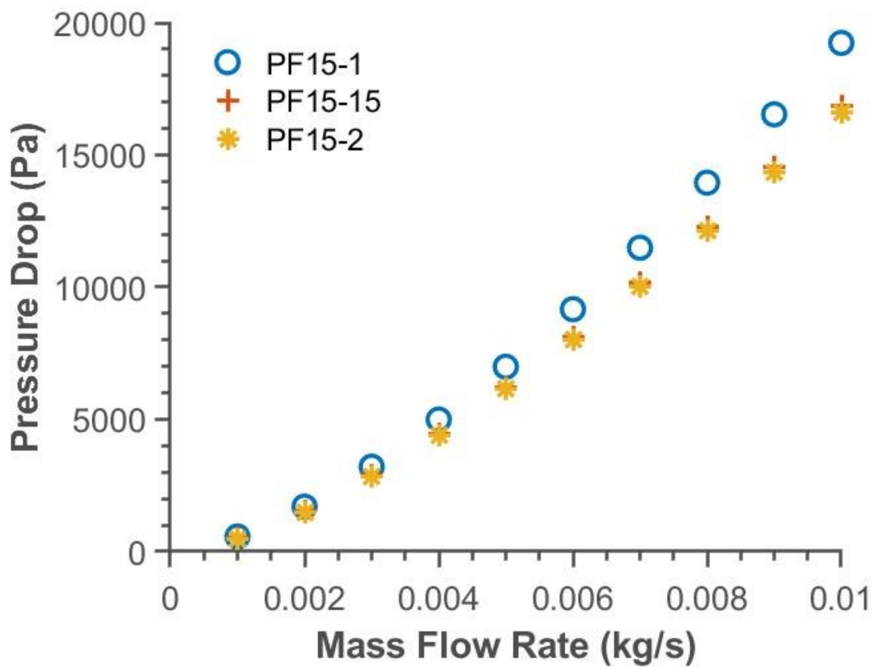

Figure 4.14: Pressure drop vs. mass flow rate for pin fin heat sink with 1.5mm diameter and 1mm, 1.5mm, and 2mm spacing.

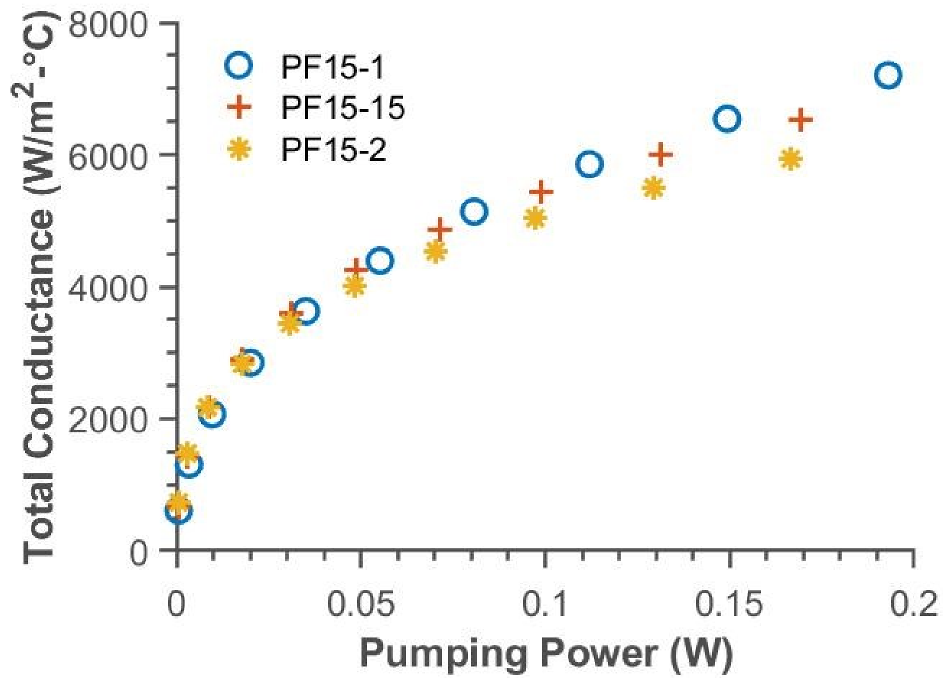

Figure 4.15: Total thermal conductance vs. pumping power for pin fin heat sink with 1.5mm diameter and 1mm, 1.5mm, and 2mm spacing.

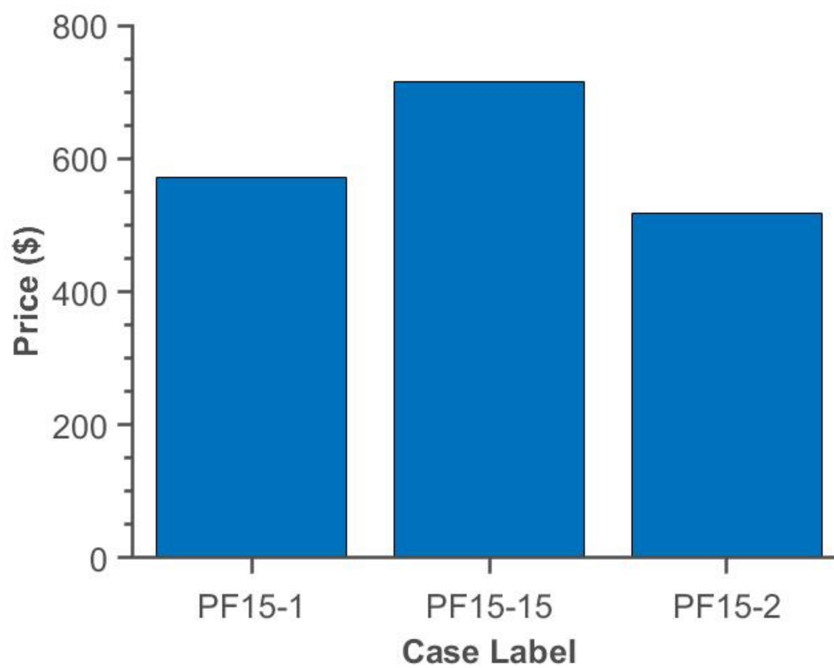

Figure 4.16: Prices for pin fin heat sink with 1.5mm diameter and 1mm, 1.5mm, and 2mm spacing.

4.2.4 Pin Fin Varying Diameter: 1mm Spacing

Figure 4.17 shows the total thermal conductance vs. mass flow rate for the pin fin heat sinks with 1mm spacing and 0.5mm, 1mm, and 1.5mm diameter. At low flow rates, the G values are close for all three cases. At flow rates starting at 0.006kg/s and above, the PF1-1 and PF15-1 overtake the PF05-1 design in G value, but not significantly. This can be explained by the fact that the PF05-1 design has the same spacing of fins, but less fin material than the other two cases, since the diameter is smaller. This smaller diameter translates to less surface area for heat transfer to occur between the pin and fluid, which ultimately results in the lower G values seen in this figure. Also of note is how close the PF1-1 and PF15-1 designs are in G value at all flow rates. This seems to indicate a diameter size between 0.5mm and 1mm at which diminishing returns of improved heat transfer occurs. Also of note is that starting at a flow rate of 0.003kg/s, all cases achieve a G value of 2000 W/m^2-ºC. This indicates that at this flow rate and higher, all cases will cool the Keysight Technologies circuit board adequately.

Figure 4.18 shows the pressure drop vs. mass flow rate for the pin fin heat sinks with 1mm spacing and 0.5mm, 1mm, and 1.5mm diameter. At flow rates lower than 0.006kg/s, the pressure drops are close in all three cases. At flow rates of 0.006kg/s and higher, the pressure drops diverge with the PF1-1 and PF15-1 designs having higher pressure drops than PF05-1. This trend is like these cases' trend in G values, where the PF1-1 and PF15-1 cases have similar pressure drop values but both being higher than PF05-1. It can also be seen that there is a trend of higher pressure drop in designs with larger pin fin diameters, especially at flow rates above 0.006kg/s. This can be explained by the fact that the larger pin fin diameter translates to less space for the fluid to flow across the entirety of the flow area.

Figure 4.19 shows the total thermal conductance vs. pumping power for the pin fin heat sinks with 1mm spacing and 0.5mm, 1mm, and 1.5mm diameter. The figure shows that having

higher G values incurs the price of having higher pumping power values, both between cases and for the same case between different mass flow rates as well. More importantly, Figure 4.19 illustrates that in practical terms, the three heat sinks considered have the same overall performance; thus, the manufacturing cost would be the defining factor for choosing a heat sink among these designs.

Figure 4.20 shows prices for the pin fin heat sink with 1mm spacing and 0.5mm, 1mm, and 1.5mm diameter. The prices go in order of lowest to highest of PF15-1, PF1-1, and PF05-1. This trend of increasing price with decreasing pin diameter is easily explained by the fact that machining smaller diameter pin fins will require smaller tooling and longer machining time, which translates directly into higher manufacturing cost.

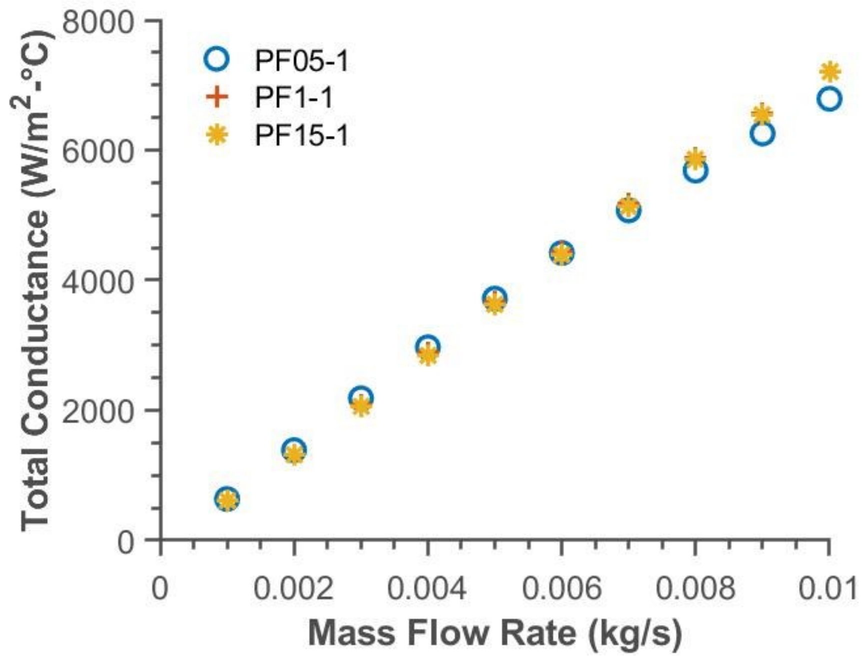

Figure 4.17: Total thermal conductance vs. mass flow rate for pin fin heat sink with 1mm spacing and 0.5mm, 1mm, and 1.5mm diameter.

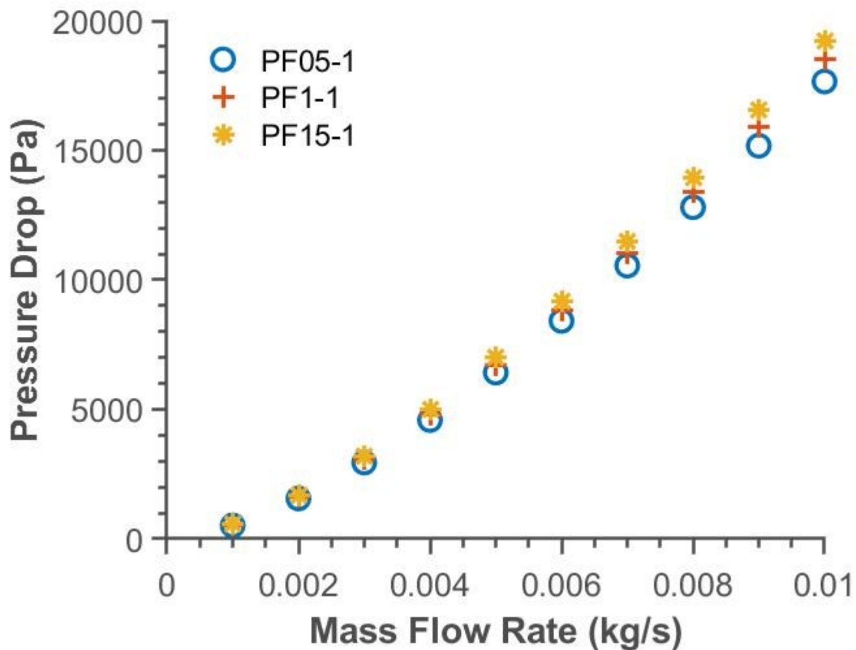

Figure 4.18: Pressure drop vs. mass flow rate for pin fin heat sink with 1mm spacing and 0.5mm, 1mm, and 1.5mm diameter.

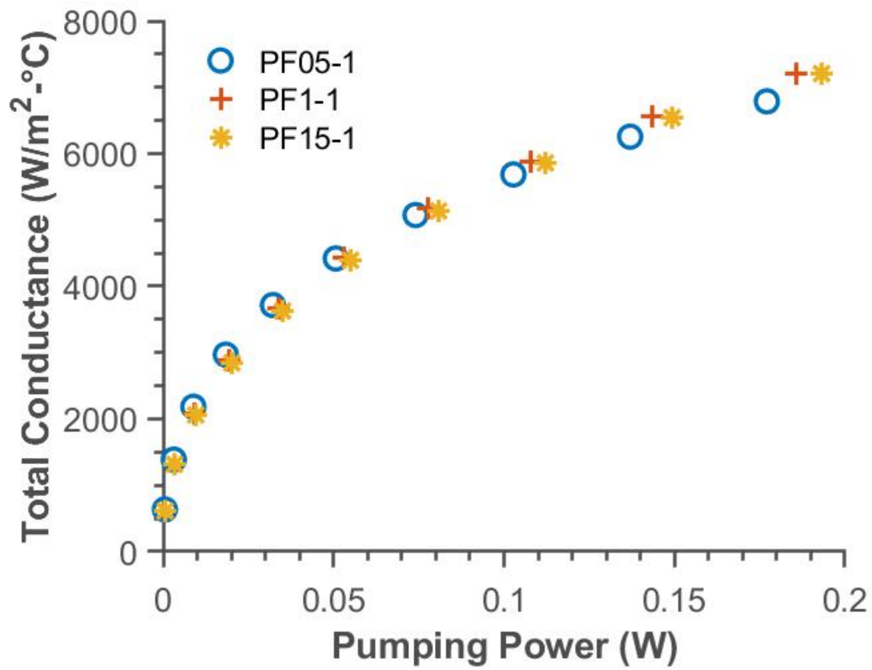

Figure 4.19: Total thermal conductance vs. pumping power for pin fin heat sink with 1mm spacing and 0.5mm, 1mm, and 1.5mm diameter.

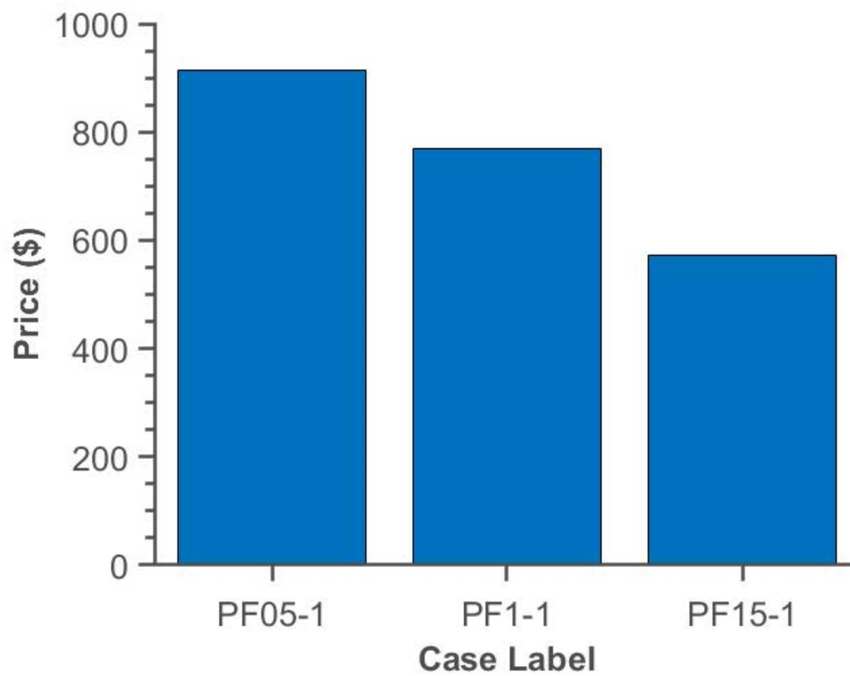

Figure 4.20: Prices for pin fin heat sink with 1mm spacing and 0.5mm, 1mm, and 1.5mm diameter

4.2.5 Pin Fin Varying Diameter: 1.5mm Spacing

Figure 4.21 shows the total thermal conductance vs. mass flow rate for the pin fin heat sinks with 1.5mm spacing and 0.5mm, 1mm, and 1.5mm diameter. At mass flow rates below 0.004kg/s, the G values for the three cases are very close. At flow rates at and above 0.004kg/s, the G values trend higher with increased diameter. Similarly to section 4.2.4, this can be explained with the fact that smaller diameter translates to less surface area for heat transfer to occur between the pin and fluid, which ultimately resulting in lower G values than larger diameters pin designs. Unlike Section 4.2.4, increasing the spacing between the fins created a more noticeable effect of the fin size on G. Also of note is that starting at a flow rate of 0.003kg/s, all cases achieve a G value of 2000 W/m^2-ºC. This indicates that at this flow rate and higher, all cases will cool the Keysight Technologies circuit board adequately.

Figure 4.22 shows the pressure drop vs. mass flow rate for the pin fin heat sinks with 1.5mm spacing and 0.5mm, 1mm, and 1.5mm diameter. While the pressure drops of the three cases are close across all flow rates, there is a trend starting at 0.006kg/s of slightly increased pressure drop with increased fin diameter. Similar to section 4.2.4, this can be explained by the fact that the larger pin fin diameter translates to less space for the fluid to flow across the entirety of the flow area, driving the pressure up. However, it is useful to note that the 1.5mm spacing of this section causes a less dramatic pressure difference between pin diameters than that of the 1mm spacing examined in section 4.2.4. This indicates that the further the pins are spaced out, the less effect the diameter size has on pressure drop of the heat sink.

Figure 4.23 shows the total thermal conductance vs. pumping power for the pin fin heat sinks with 1.5mm spacing and 0.5mm, 1mm, and 1.5mm diameter. The figure shows a similar trend to the previous section. However, it is interesting to note that the two larger diameter cases have a higher G value with a lower pumping power cost than in the previous 1mm spacing

section. Unlike the results in Section 4.2.4, the differences between the overall performance of the heat sinks are clearer.

Figure 4.24 shows the prices for the pin fin heat sinks with 1.5mm spacing and 0.5mm, 1mm, and 1.5mm diameter. The cases in order from lowest to highest price are PF05-15, PF15-15, and PF1-15.

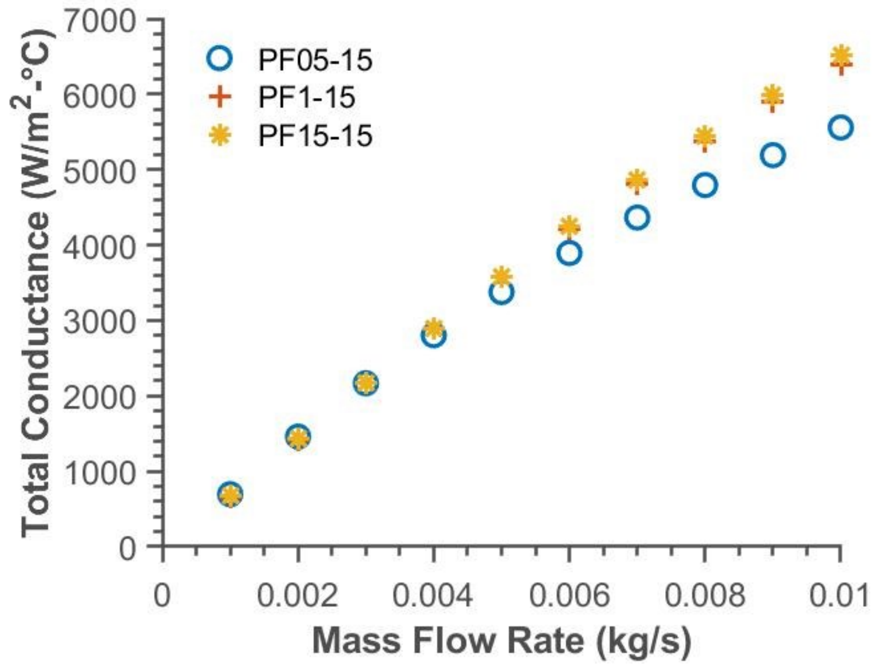

Figure 4.21: Total thermal conductance vs. mass flow rate for pin fin heat sink with 1.5mm spacing and 0.5mm, 1mm, and 1.5mm diameter.

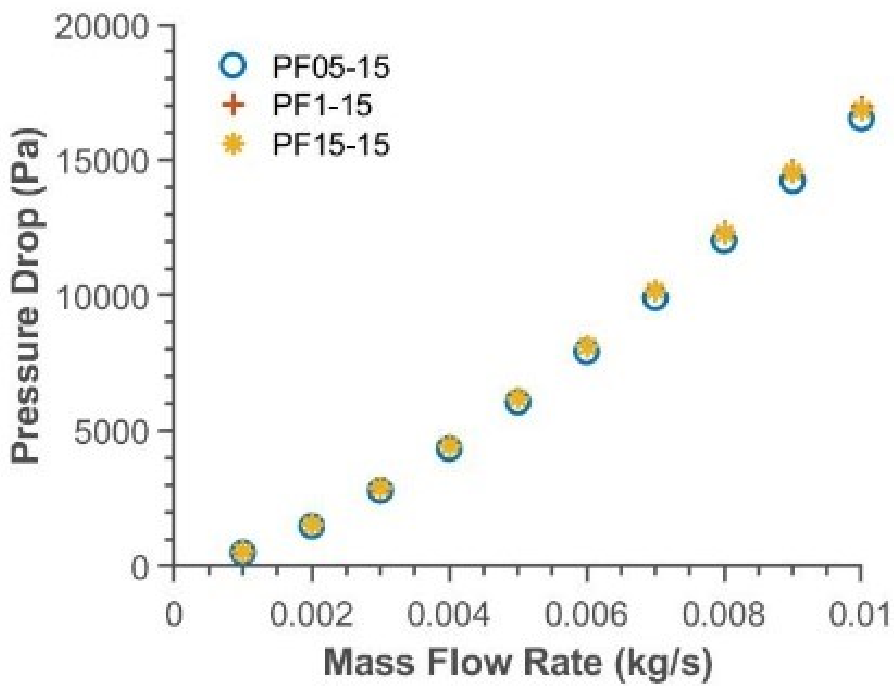

Figure 4.22: Pressure drop vs. mass flow rate for pin fin heat sink with 1.5mm spacing and 0.5mm, 1mm, and 1.5mm diameter

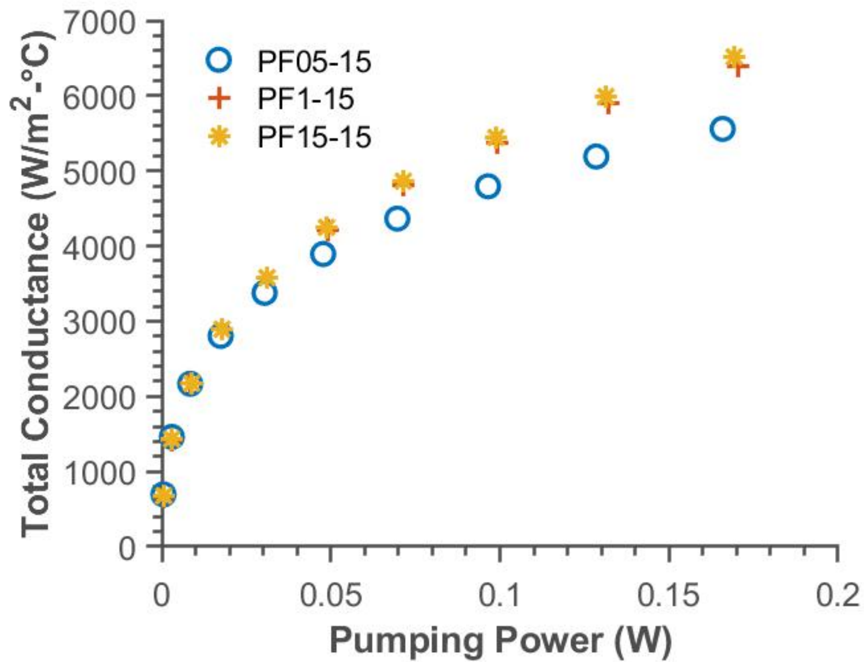

Figure 4.23: Total thermal conductance vs. pumping power for pin fin heat sink with 1.5mm spacing and 0.5mm, 1mm, and 1.5mm diameter.

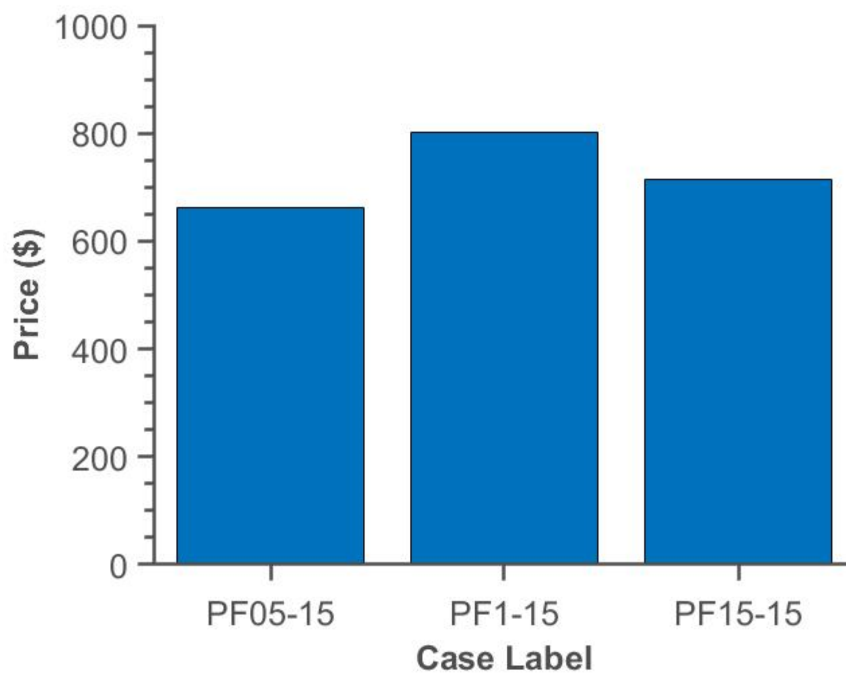

Figure 4.24: Prices for pin fin heat sink with 1.5mm spacing and 0.5mm, 1mm, and 1.5mm diameter.

4.2.6 Pin Fin Varying Diameter: 2mm Spacing

Figure 4.25 shows the total thermal conductance vs. mass flow rate for the pin fin heat sinks with 2mm spacing and 0.5mm, 1mm, and 1.5mm diameter. Similar to the trends of the previous two sections, G tends to increase with increasing pin diameter. This trend begins at a flow rate at 0.003kg/s and continues at all higher flow rates. Before 0.003kg/s, the G values are similar across all three cases. Similar to the previous to sections, this can be explained with the fact that smaller pin diameter translates to less surface area for heat transfer to occur between the pin and fluid, which results in lower G values than larger diameters pin designs. Of note in this section is the fact that the two larger diameter pin cases have markedly different G values, whereas in the previous two sections the G values of the two larger diameter pin cases were nearly the same. This indicates that as spacing is increased, the effect of the pin diameter on the total thermal conductance increases. Also of note is that starting at a flow rate of 0.003kg/s, all cases achieve a G value of 2000 W/m^2-ºC. This indicates that at this flow rate and higher, all cases will cool the Keysight Technologies circuit board adequately.

Figure 4.26 shows the pressure drop vs. mass flow rate for the pin fin heat sinks with 2mm spacing and 0.5mm, 1mm, and 1.5mm diameter. While the pressure drops of the three cases are close across all flow rates, there is a trend starting at 0.005kg/s of slightly increased pressure drop with increased fin diameter. Like the previous two sections, this can be explained by the fact that the larger pin fin diameter translates to less space for the fluid to flow across the entirety of the flow area, driving the pressure losses up. The trend noted in the previous section of further pin spacing causing less dramatic pressure difference between pin diameters persists in this section as well, confirming that the further the pins are spaced out, the less effect the diameter size has on pressure drop of the heat sink.

Figure 4.27 shows the total thermal conductance vs. pumping power for the pin fin heat sinks with 2mm spacing and 0.5mm, 1mm, and 1.5mm diameter. The figure shows a similar trend to the previous two sections, with increasing G requiring increasing pumping power. Similar to the previous section, it is of note that the two larger diameter cases have a higher G value with a lower pumping power cost than in the 1mm spacing section, and slightly higher G values with lower pumping power cost than in the 1.5mm spacing section. Unlike the previous Section, more noticeable differences are observed between the overall performance calculations of the heat sinks. This is due to the marked effect of the fin diameter on G at a spacing of 2 mm.

Figure 4.28 shows the prices for the pin fin heat sinks with 2mm spacing and 0.5mm, 1mm, and 1.5mm diameter. The cases in order of lowest to highest price are PF1-2, PF05-2, and PF15-2.

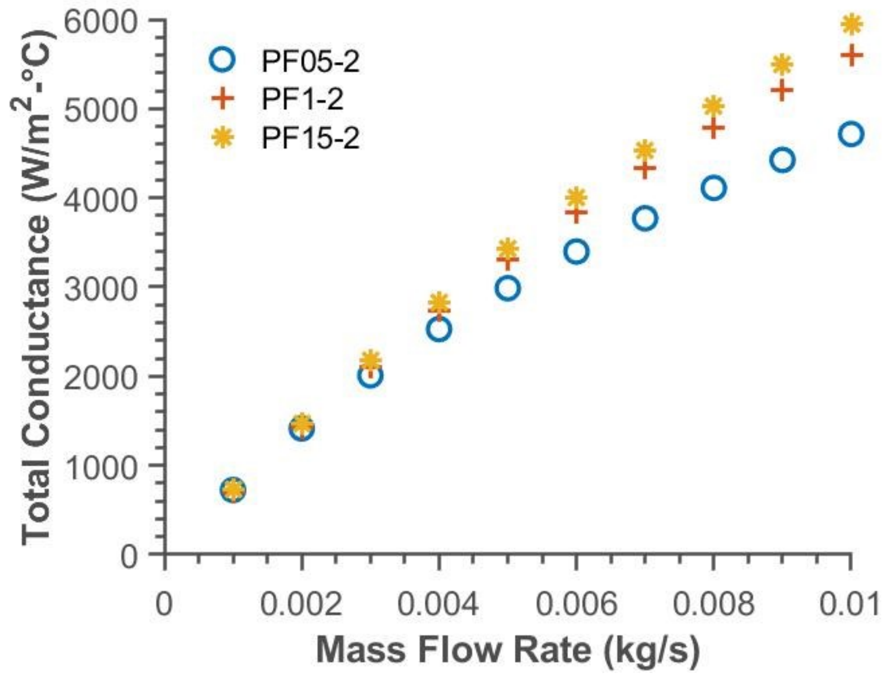

Figure 4.25: Total thermal conductance vs. mass flow rate for pin fin heat sink with 2mm spacing and 0.5mm, 1mm, and 1.5mm diameter.

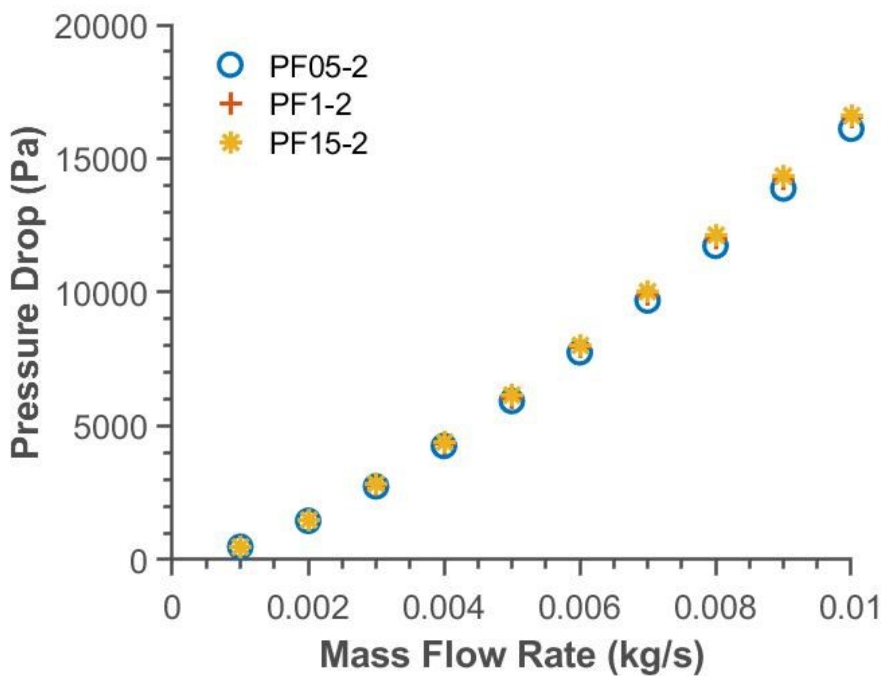

Figure 4.26: Pressure drop vs. mass flow rate for pin fin heat sink with 2mm spacing and 0.5mm, 1mm, and 1.5mm diameter

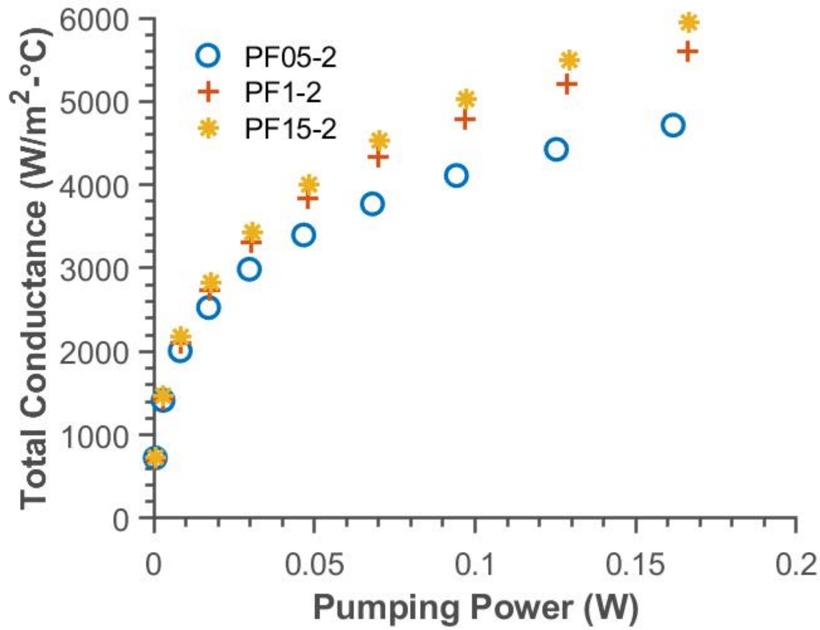

Figure 4.27: Total thermal conductance vs. pumping power for pin fin heat sink with 2mm spacing and 0.5mm, 1mm, and 1.5mm diameter.

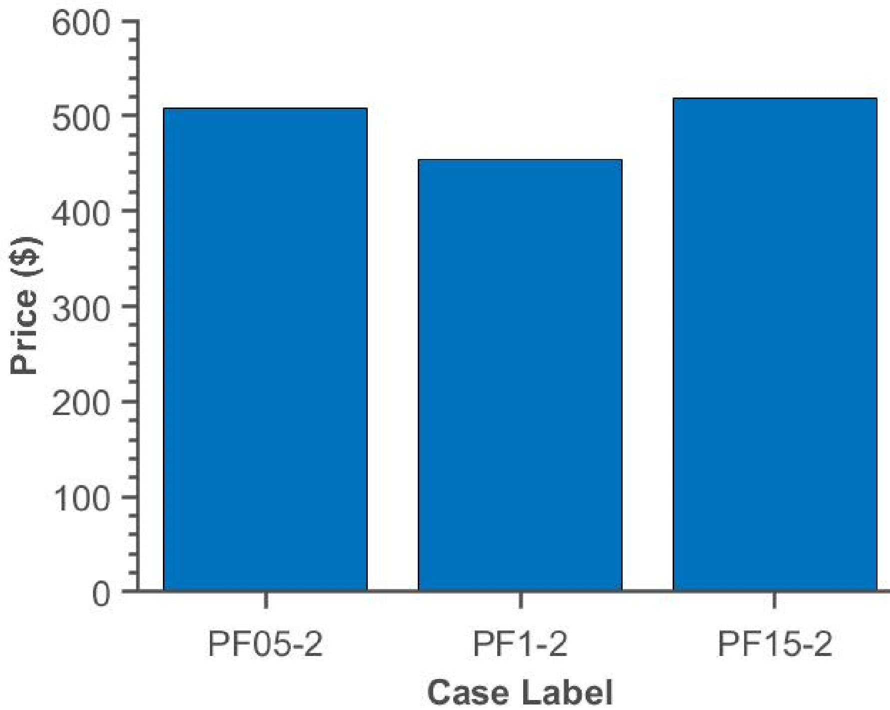

Figure 4.28: Prices for pin fin heat sink with 2mm spacing and 0.5mm, 1mm, and 1.5mm diameter.

4.3 Channel Design

This section involves the presentation and discussion of the MCLF (mini channel long fin) and MCSF (mini channel short fin) heat sink designs. See Figures 3.8 and 3.9 for these design's geometries.

Figure 4.29 shows the total thermal conductance vs. mass flow rate for the mini channel heat sink with 1mm spacing and long and short fins. Across almost all mass flow rates, except 0.01kg/s, the MCSF design has a slightly better total thermal conductance than the MCLF design. One reason for this is that the MCSF design allows for better flow distribution across all channels. In contrast, the MCLF design forces fluid to flow mainly through the middle several channels, producing slow fluid flow through the peripheral channels and causing less heat transfer overall. Also of note is that starting at a flow rate of 0.003kg/s, both cases achieve a G value of 2000 W/m^2-°C. This indicates that at this flow rate and higher, both cases will cool the Keysight Technologies circuit board adequately.

Figure 4.30 shows the pressure drop vs. mass flow rate for the mini channel heat sink with 1mm spacing and long and short fins. Across all flow rates, the MCLF has higher pressure drop than the MCSF. This can be explained by the fact that the MCLF has much longer channels for the fluid to flow through than the MCSF, causing more friction losses. The differences between the pressure drops of the two cases increases and mass flow rate increases.

Figure 4.31 shows the total thermal conductance vs. pumping power for mini channel heat sink with 1mm spacing and long and short fins. This figure shows the tradeoffs between total thermal conductance and pumping power for the designs. In previous sections, most designs that had better thermal conductance required more pumping power as a cost. In this section, the MCSF outperforms the MCLF in pumping power requirements, while the thermal performance is

quite similar. The reasons for this are explained in the paragraphs above and amount to the longer fins of the MCLF causing higher pressure drop.

Figure 4.32 shows the price for the mini channel heat sink with 1mm spacing and long and short fins. It shows that the MCSF is cheaper in price than the MCLF. This is most likely due to the fact that the MCLF requires more features to be machined out, requiring more machining time than the MCSF which translates directly to higher manufacturing cost. In contrast to previous sections and design comparisons in this thesis, the MCSF surpasses the MCLF in all categories: thermal conductance, pumping power and manufacturing price.

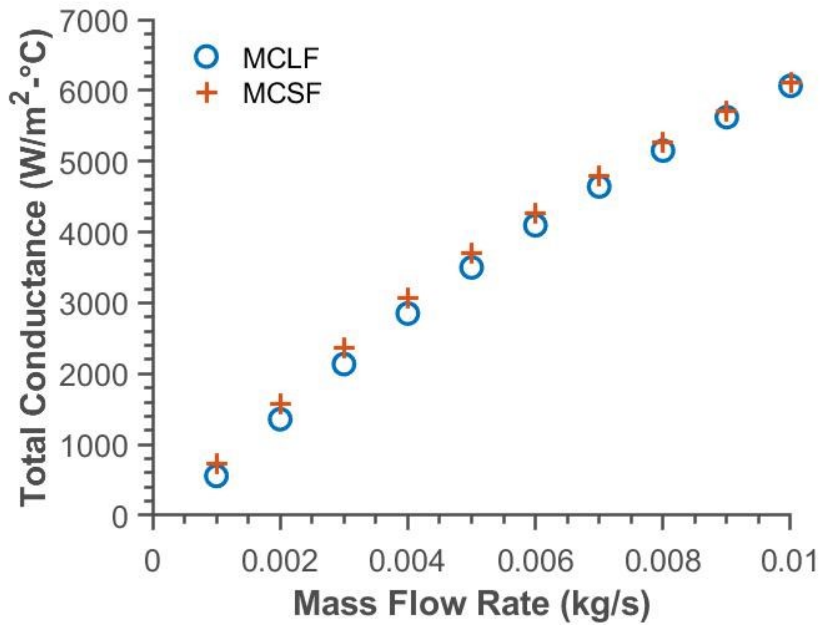

Figure 4.29: Total thermal conductance vs. mass flow rate for mini channel heat sink with 1mm spacing and long and short fins.

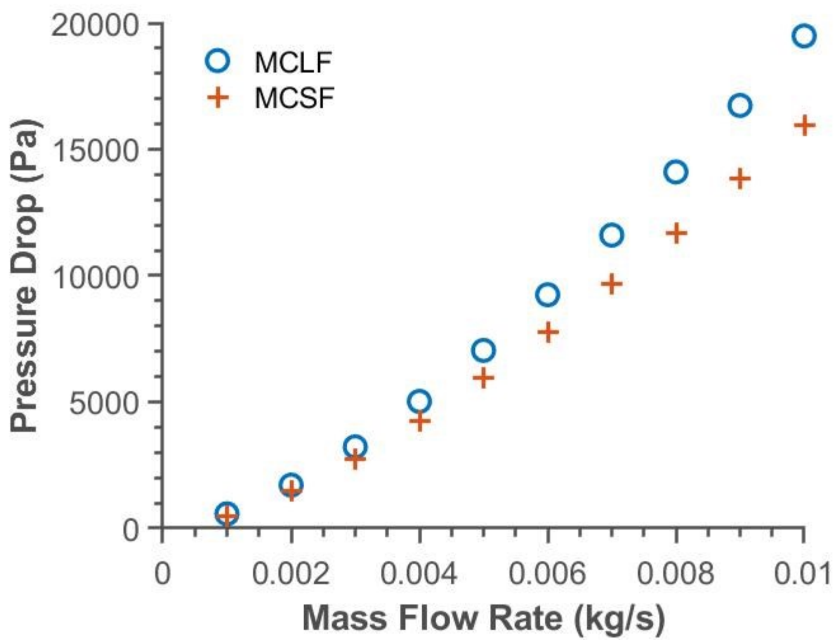

Figure 4.30: Pressure drop vs. mass flow rate for mini channel heat sink with 1mm spacing and long and short fins.

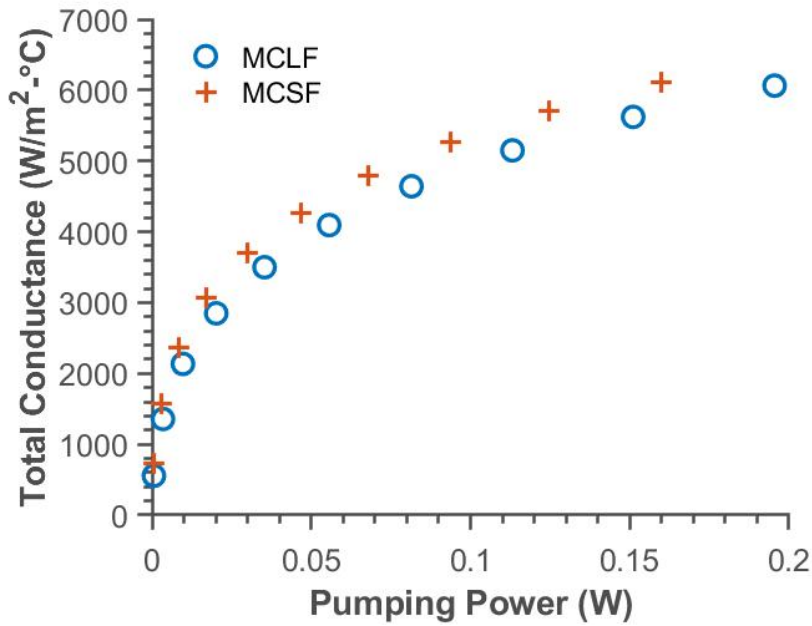

Figure 4.31: Total thermal conductance vs. pumping power for mini channel heat sink with 1mm spacing and long and short fins.

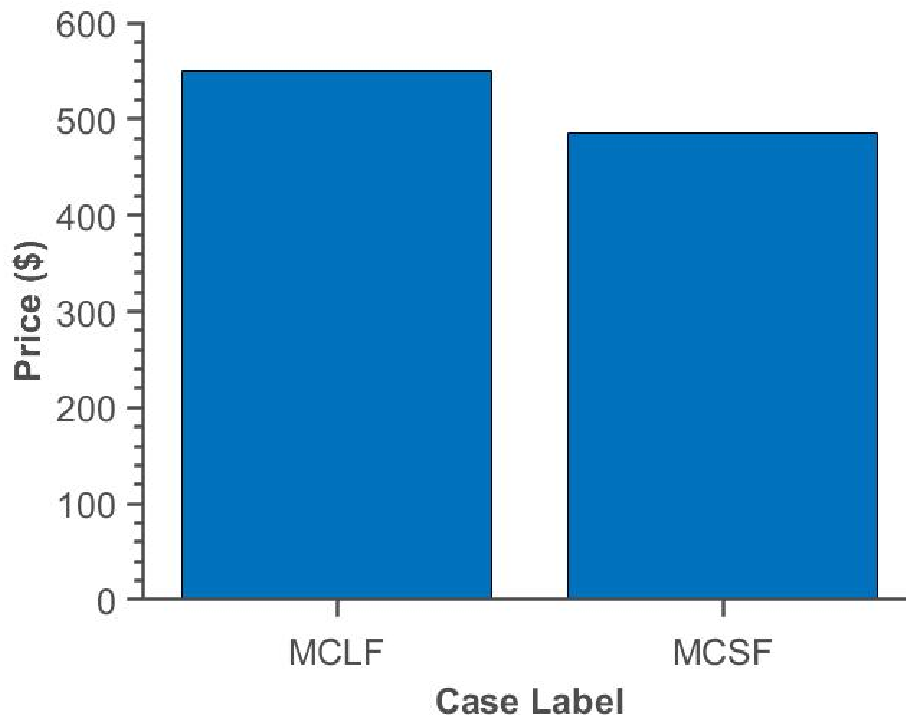

Figure 4.32: Price for mini channel heat sink with 1mm spacing and long and short fins.

4.4 Select Designs with Aluminum

Recall that all cases in previous sections of Chapter 4 achieved a total thermal conductance (G) value of 2000 W/m^2-ºC starting at a flow rate of 0.003kg/s. This indicates that at this low flow rate and higher, all cases will cool the Keysight Technologies circuit board adequately. This also indicates that a measure of optimization can occur with the designs, since the minimum value of G = 2000 W/m^2-ºC is achieved at rather low flow rates with copper plate heat sinks. The author has chosen to examine optimization in the form of changing the material from copper to aluminum for two select heat sink designs. This will cause a lower thermal conductance value due to the lower thermal conductivity of aluminum versus copper, but will allow for more cost savings in manufacturing since aluminum is cheaper than copper. The two designs selected were the PF1-1 and MCSF because they are representative of the two types of designs this thesis focuses on, one being a pin fin design and one being a mini channel design. This section reports and discusses the results of the aluminum heat sink simulations. Note that pressure drop is not reported here, since a material change will not affect the pressure drop.

Figure 4.33 shows total thermal conductance vs. mass flow rate for the heat sink designs PF1-1 and MCSF in copper material compared with aluminum material. As predicted, the aluminum heat sinks have lower G values than the copper ones, although only by approximately 150 W/m^2-ºC. The aluminum designs still achieve G values of 2000 W/m^2-ºC at a flow rate of 0.003kg/s, and continuously higher G values at higher flow rates.

Figure 4.34 shows the total thermal conductance vs. pumping power for the heat sink designs PF1-1 and MCSF in copper material compared with aluminum material. As expected, this

figure simply shows that the aluminum designs gain less G value for the pumping power price than their copper counterparts.

Figure 4.35 shows the prices for the heat sink designs PF1-1 and MCSF in copper material compared with aluminum material. As predicted, the aluminum heat sinks are significantly cheaper than their copper versions- approximately 30% cheaper.

In summary, changing the material from copper to aluminum was a good optimization choice, since the G values were not lowered enough to affect the designs' ability to cool the Keysight Technologies circuit board, and the aluminum designs are approximately 30% cheaper than the copper ones.

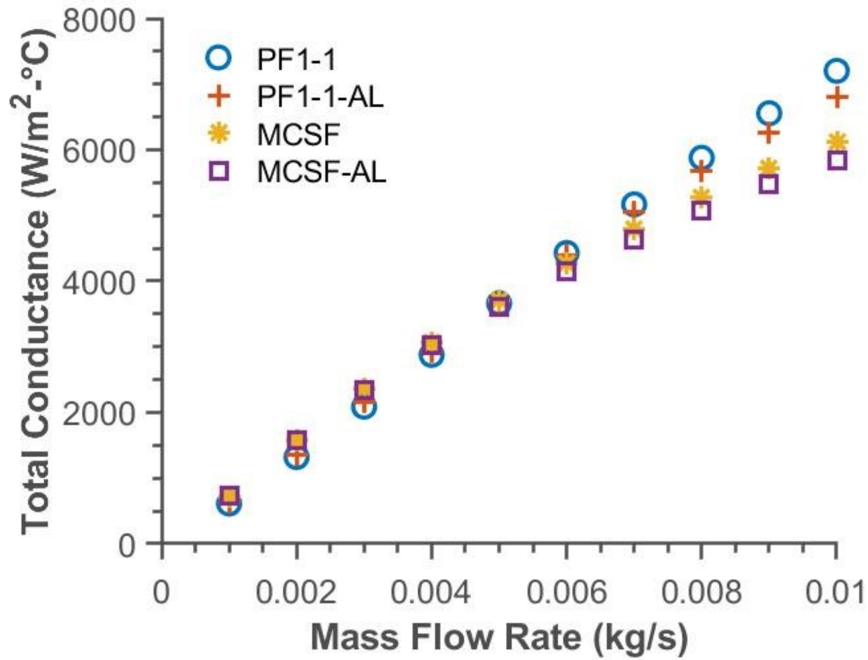

Figure 4.33: Total thermal conductance vs. mass flow rate for heat sink designs PF1-1 and MCSF in copper material compared with aluminum material.

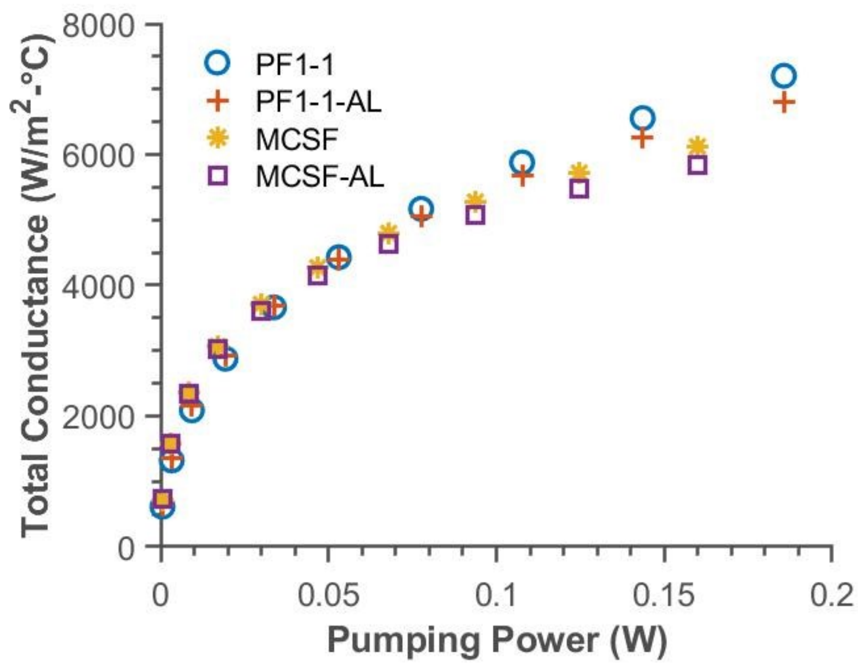

Figure 4.34: Total thermal conductance vs. pumping power for heat sink designs PF1-1 and MCSF in copper material compared with aluminum material.

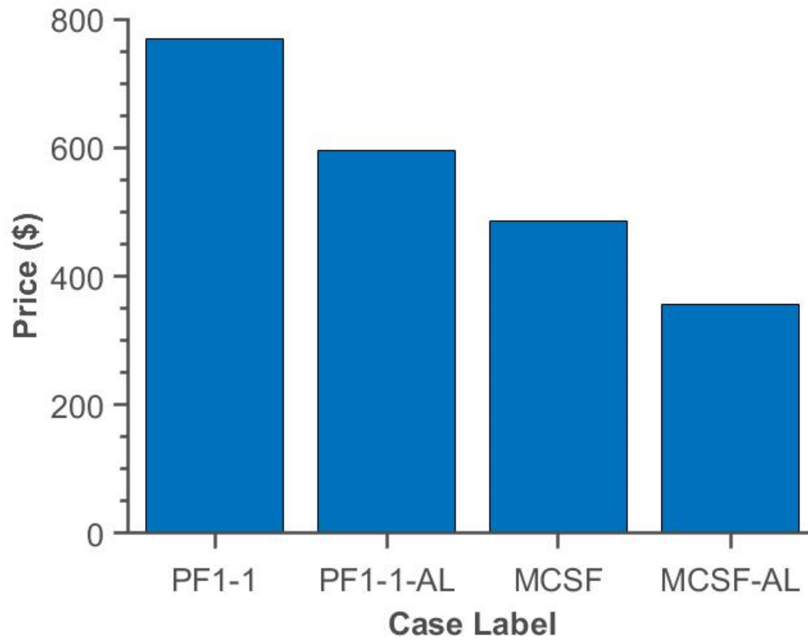

Figure 4.35: Prices for heat sink designs PF1-1 and MCSF in copper material compared with aluminum material

4.5 Combined Performance Parameter PPTC and PPTC/Dollar

To compare the simulation cases directly, the author has formulated an overall performance evaluation metric called Pumping-Power-Thermal-Conductance (PPTC). This parameter was inspired by Paniagua-Guerra and Ramos-Alvarado[47], who used a Pumping Power Thermal Resistance (PPTR) parameter. The PPTC parameter is found by curve fitting a given case's total thermal conductance versus pumping power simulation data and integrating the area under the curve, this allows to generate a single-number metric to assess the overall performance of a liquid-cooled heat sink. The PPTC is inspired on the idea that the higher a dataset is on a G vs pumping power plot, the better the overall performance; hence, the higher the PPTC value, the better the overall heat sink's performance. To allow for a fair comparison, all pumping power axes were truncated to 0.2W during the curve fitting. Also, the pumping power

range was normalized by dividing by 0.2W to give the PPTC the same units as G for convenience. Figure 4.36 and 4.37 show examples of the curve fits found. This PPTC parameter thus considers both the thermal characteristics and hydrodynamic characteristics of the given case. Once the PPTC is found in this way, it can be divided by the dollar price of the heat sink to give an overall comparison parameter of PPTC/dollar. Each case's PPTC/dollar amount can be directly compared to each other, taking the price, thermal characteristics, and hydrodynamic characteristics into account with one single parameter.

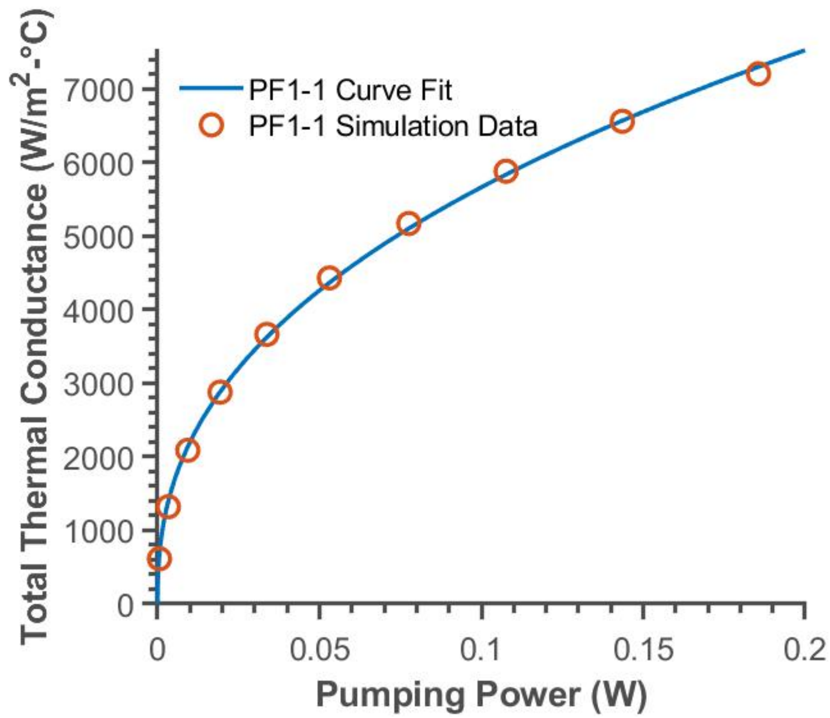

Figure 4.36: The best curve fit found for case PF1-1 simulation data.

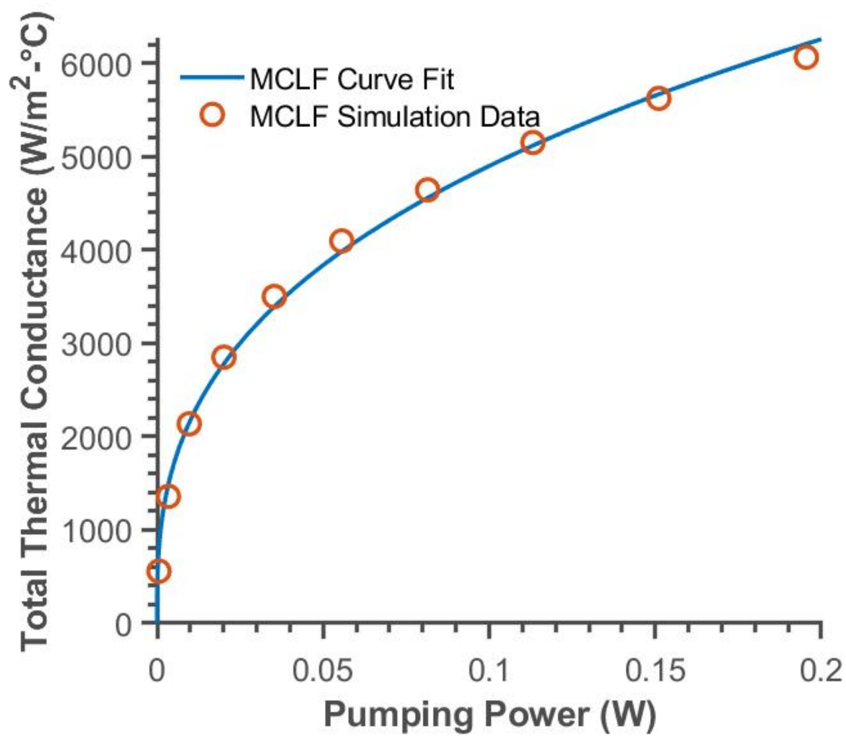

Figure 4.37: The best curve fit found for case MCLF simulation data.

Figure 4.38 shows the PPTC of each case. This figure shows that the cases with the top three PPTC values, in order from highest to lowest, are MCSF, MCSF-AL, and PF05-1. This means that out of all the cases, these three are the ones with the combined highest heat transfer and best hydraulic (overall) performance. Figure 4.39 shows the PPTC/$ of each case. Recall that this figure effectively shows each case's overall (combined hydraulic and heat transfer) performance per dollar spent. The figure shows that the cases with the top three PPTC/$ values, in order from highest to lowest, are MCSF-AL, MCSF, and PF1-2. This means that out of all the cases, these three are the ones with the combined highest heat transfer, best hydraulic performance and lowest manufacturing price.

Comparing figure 4.38 and figure 4.39, it is apparent why the PPTC and PPTC/$ metrics are distinct and effective in different situations. The ordering of which case is preferable changes dramatically once manufacturing price is involved. In situations where the raw heat transfer and hydraulic performance are of prime importance, the PPTC shown in figure 4.38 can be used. If manufacturing cost is important, then the PPTC/$ can better offer insight into which design is preferable.

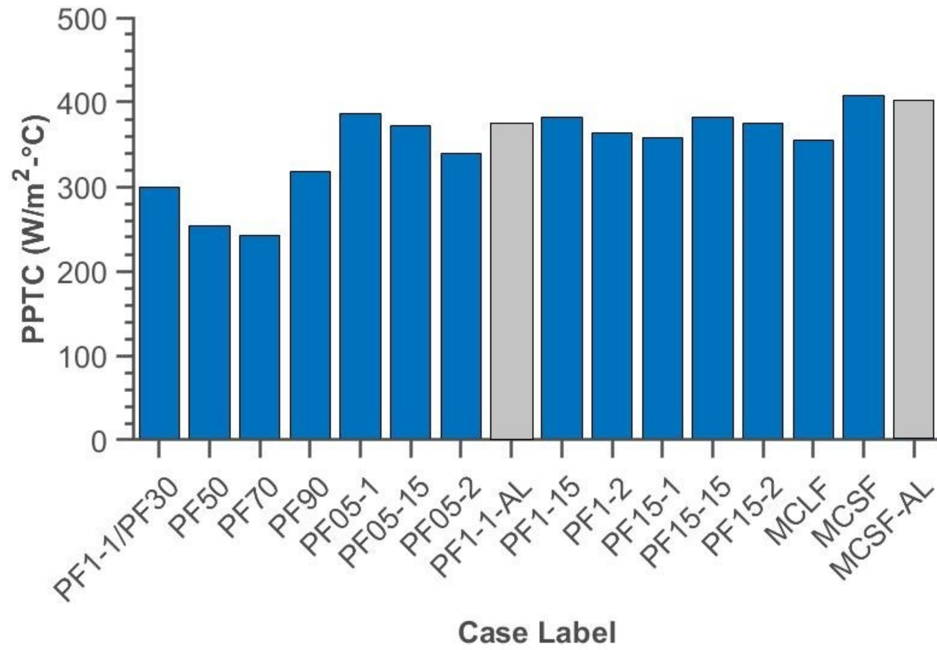

Figure 4.38: Pumping power thermal conductivity (PPTC), a combined comparison parameter of each case, copper designs in blue and aluminum designs in grey.

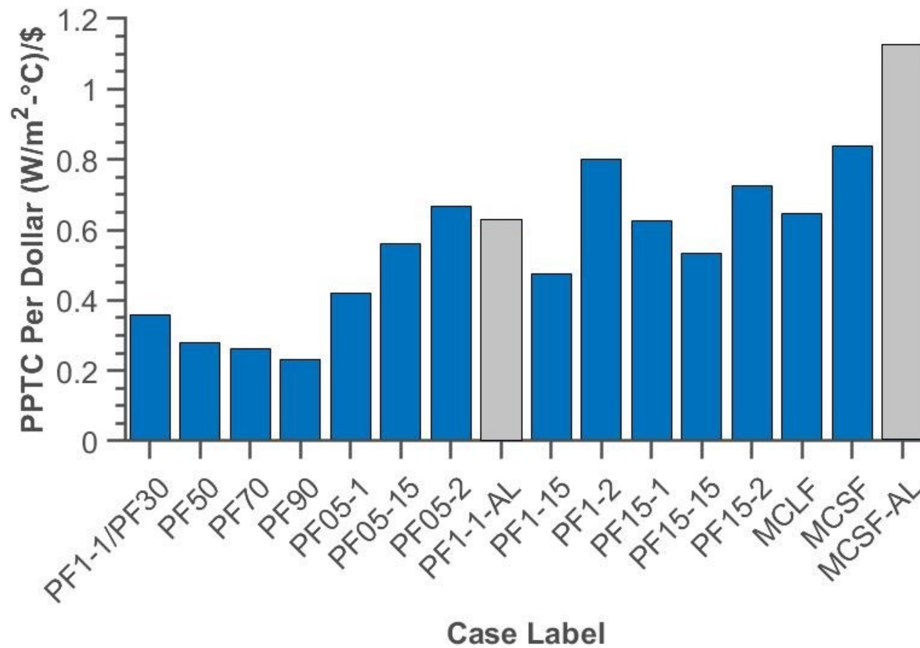

Figure 4.39: Pumping power thermal conductivity (PPTC) per dollar, a combined comparison parameter of each case divided by the case's dollar cost, copper designs in blue and aluminum designs in grey.

Chapter 5
Conclusion

5.1 Summary and Conclusions

In conclusion, the problem of cooling Keysight Technologies' circuit board using liquid cooling was the focus of this thesis. The approach was to examine the effect on performance and price of three common design features of liquid cooling heat sinks: the header angle, pin fin geometry, and mini channel geometry. Specifically, the effect of diameter and spacing of the pin fin geometry and the effect of length of the mini channel geometry were examined. The methods used were that of numerical CFD simulation using the Ansys Fluent 19.2 software package. The system's geometry was modeled using 3D modeling software and set up for simulation in Ansys Fluent using the appropriate boundary conditions of the physical system. The simulations yielded raw pressure and temperature data, which were processed into a combined heat transfer and hydraulic performance parameter PPTC. Since this was a real-world application to be used for purchasing prototypes, manufacturing cost was considered using Protolabs' online auto-quoting tool. The manufacturing price was combined with the PPTC parameter to implement a PPTC/$ parameter, using which can allow comparison between each heat sink design. The economic consideration of manufacturing cost is unique because many studies focus solely on technical performance parameters and neglect the cost of fabrication. It was found that the cases with the top three PPTC/$ values, in order from highest to lowest, are MCSF-AL (mini channel short fin-aluminum), MCSF (mini channel short fin-copper), and PF1-2 (Pin fin, 1mm diameter, 1mm spacing-copper).

5.2 Future Work

There is much future work to be done following this thesis. Primarily this future work is experimental validation of the simulation results found here. Parts have already been purchased to allow the proper experimentation, and three plate designs have been purchased from Protolabs for testing (PF1-1, PF1-2, and MCSF), all in aluminum based on the findings of the simulations. These plates will be subjected to different heating loads and will eventually be tested on the Keysight Technologies circuit board, and the system will be measured to see if the designs do indeed cool the chips adequately, as is predicted by the simulations in this thesis.

References

[1] B. R. Mahajan, C. Chiu, and G. Chrysler, "Cooling a Microprocessor Chip," vol. 94, no. 8, 2006.

[2] M. Pedram and S. Nazarian, "Thermal modeling, analysis, and management in VLSI circuits: Principles and methods," *Proc. IEEE*, vol. 94, no. 8, pp. 1487–1501, 2006, doi: 10.1109/JPROC.2006.879797.

[3] Z. Khattak and H. M. Ali, "Air cooled heat sink geometries subjected to forced flow: A critical review," *Int. J. Heat Mass Transf.*, vol. 130, pp. 141–161, 2019, doi: 10.1016/j.ijheatmasstransfer.2018.08.048.

[4] R. W. Keyes, "Physical Limits in Digital Electronics," vol. 63, no. 5, 1975.

[5] A. Baïri, J. M. García De María, I. Baïri, N. Laraqi, E. Zarco-Pernia, and N. Alilat, "2D transient natural convection in diode cavities containing an electronic equipment with discrete active bands under constant heat flux," *Int. J. Heat Mass Transf.*, vol. 55, no. 19–20, pp. 4970–4980, 2012, doi: 10.1016/j.ijheatmasstransfer.2012.04.032.

[6] A. Baudoin, D. Saury, and C. Boström, "Optimized distribution of a large number of power electronics components cooled by conjugate turbulent natural convection," *Appl. Therm. Eng.*, vol. 124, pp. 975–985, 2017, doi: 10.1016/j.applthermaleng.2017.06.058.

[7] P. M. Teertstra, M. M. Yovanovich, and J. R. Culham, "Modeling of natural convection in electronic enclosures," *J. Electron. Packag. Trans. ASME*, vol. 128, no. 2, pp. 157–165, 2006, doi: 10.1115/1.2188953.

[8] E. M. Sparrow, J. W. Ramsey, and C. A. C. Altemani, "Experiments on in-line pin fin arrays-and performance comparisons with staggered arrays," *J. Heat Transfer*, vol. 102, no. 1, pp. 44–50, 1980, doi: 10.1115/1.3244247.

[9] Y. Peles, A. Koşar, C. Mishra, C. J. Kuo, and B. Schneider, "Forced convective heat transfer across a pin fin micro heat sink," *Int. J. Heat Mass Transf.*, vol. 48, no. 17, pp. 3615–3627, 2005, doi: 10.1016/j.ijheatmasstransfer.2005.03.017.

[10] A. Mohammed Adham, N. Mohd-Ghazali, and R. Ahmad, "Thermal and hydrodynamic analysis of microchannel heat sinks: A review," *Renew. Sustain. Energy Rev.*, vol. 21, pp. 614–622, 2013, doi: 10.1016/j.rser.2013.01.022.

[11] H. Y. Zhang, D. Pinjala, T. N. Wong, K. C. Toh, and Y. K. Joshi, "Single-phase liquid

cooled microchannel heat sink for electronic packages," *Appl. Therm. Eng.*, vol. 25, no. 10, pp. 1472–1487, 2005, doi: 10.1016/j.applthermaleng.2004.09.014.

[12] M. E. Steinke and S. G. Kandlikar, "Single-phase heat transfer enhancement techniques in microchannel and minichannel flows," *Proc. Second Int. Conf. Microchannels Minichannels*, pp. 141–148, 2004, doi: 10.1115/icmm2004-2328.

[13] T. G. Karayiannis and M. M. Mahmoud, "Flow boiling in microchannels: Fundamentals and applications," *Appl. Therm. Eng.*, vol. 115, pp. 1372–1397, 2017, doi: 10.1016/j.applthermaleng.2016.08.063.

[14] D. Bogojevic, K. Sefiane, A. J. Walton, H. Lin, and G. Cummins, "Two-phase flow instabilities in a silicon microchannels heat sink," *Int. J. Heat Fluid Flow*, vol. 30, no. 5, pp. 854–867, 2009, doi: 10.1016/j.ijheatfluidflow.2009.03.013.

[15] A. E. Bergles and S. G. Kandlikar, "On the nature of critical heat flux in microchannels," *J. Heat Transfer*, vol. 127, no. 1, pp. 101–107, 2005, doi: 10.1115/1.1839587.

[16] S. M. Sohel Murshed and C. A. Nieto de Castro, "A critical review of traditional and emerging techniques and fluids for electronics cooling," *Renew. Sustain. Energy Rev.*, vol. 78, pp. 821–833, 2017, doi: 10.1016/j.rser.2017.04.112.

[17] S. G. Kandlikar, "High flux heat removal with microchannels - A roadmap of challenges and opportunities," *Heat Transf. Eng.*, vol. 26, no. 8, pp. 5–14, 2005, doi: 10.1080/01457630591003655.

[18] D. B. Tuckerman and R. F. W. Pease, "High-Performance Heat Sinking for VLSI," *IEEE Electron Device Lett.*, vol. EDL-2, no. 5, pp. 126–129, 1981, doi: 10.1109/EDL.1981.25367.

[19] A. Husain and K. Y. Kim, "Thermal optimization of a microchannel heat sink with trapezoidal cross section," *J. Electron. Packag. Trans. ASME*, vol. 131, no. 2, pp. 0210051–0210056, 2009, doi: 10.1115/1.3103931.

[20] A. F. Al-Neama, N. Kapur, J. Summers, and H. M. Thompson, "An experimental and numerical investigation of the use of liquid flow in serpentine microchannels for microelectronics cooling," *Appl. Therm. Eng.*, vol. 116, pp. 709–723, 2017, doi: 10.1016/j.applthermaleng.2017.02.001.

[21] S. A. Jajja, W. Ali, H. M. Ali, and A. M. Ali, "Water cooled minichannel heat sinks for microprocessor cooling: Effect of fin spacing," *Appl. Therm. Eng.*, vol. 64, no. 1–2, pp. 76–82, 2014, doi: 10.1016/j.applthermaleng.2013.12.007.

[22] X. Hao, Z. Wu, X. Chen, and G. Xie, "Numerical analysis and optimization on flow

distribution and heat transfer of a U-type parallel channel heat sink," *Adv. Mech. Eng.*, vol. 7, no. 2, 2015, doi: 10.1155/2014/672451.

[23] S. G. Kandlikar, S. Joshi, and S. Tian, "Effect of surface roughness on heat transfer and fluid flow characteristics at low Reynolds numbers in small diameter tubes," *Heat Transf. Eng.*, vol. 24, no. 3, pp. 4–16, 2003, doi: 10.1080/01457630304069.

[24] T. Bello-Ochende and A. Bejan, "Maximal heat transfer density: Plates with multiple lengths in forced convection," *Int. J. Therm. Sci.*, vol. 43, no. 12, pp. 1181–1186, 2004, doi: 10.1016/j.ijthermalsci.2004.05.002.

[25] A. F. Al-Neama, Z. Khatir, N. Kapur, J. Summers, and H. M. Thompson, "An experimental and numerical investigation of chevron fin structures in serpentine minichannel heat sinks," *Int. J. Heat Mass Transf.*, vol. 120, pp. 1213–1228, 2018, doi: 10.1016/j.ijheatmasstransfer.2017.12.092.

[26] A. A. Y. Al-Waaly, M. C. Paul, and P. Dobson, "Liquid cooling of non-uniform heat flux of a chip circuit by subchannels," *Appl. Therm. Eng.*, vol. 115, pp. 558–574, 2017, doi: 10.1016/j.applthermaleng.2016.12.061.

[27] O. Abouali and N. Baghernezhad, "Numerical investigation of heat transfer enhancement in a microchannel with grooved surfaces," *J. Heat Transfer*, vol. 132, no. 4, pp. 1–8, 2010, doi: 10.1115/1.4000862.

[28] A. Abdoli, G. Jimenez, and G. S. Dulikravich, "Thermo-fluid analysis of micro pin-fin array cooling configurations for high heat fluxes with a hot spot," *Int. J. Therm. Sci.*, vol. 90, pp. 290–297, 2015, doi: 10.1016/j.ijthermalsci.2014.12.021.

[29] A. Koşar and Y. Peles, "Thermal-hydraulic performance of MEMS-based pin fin heat sink," *J. Heat Transfer*, vol. 128, no. 2, pp. 121–131, 2006, doi: 10.1115/1.2137760.

[30] P. Naphon and S. Wiriyasart, "Liquid cooling in the mini-rectangular fin heat sink with and without thermoelectric for CPU," *Int. Commun. Heat Mass Transf.*, vol. 36, no. 2, pp. 166–171, 2009, doi: 10.1016/j.icheatmasstransfer.2008.10.002.

[31] Y. T. Yang and H. Sen Peng, "Numerical study of pin-fin heat sink with un-uniform fin height design," *Int. J. Heat Mass Transf.*, vol. 51, no. 19–20, pp. 4788–4796, 2008, doi: 10.1016/j.ijheatmasstransfer.2008.02.017.

[32] N. Sahiti, F. Durst, and P. Geremia, "Selection and optimization of pin cross-sections for electronics cooling," *Appl. Therm. Eng.*, vol. 27, no. 1, pp. 111–119, 2007, doi: 10.1016/j.applthermaleng.2006.05.018.

[33] W. A. Khan, J. R. Culham, and M. M. Yovanovich, "Performance of shrouded pin-fin heat

sinks for electronic cooling," *J. Thermophys. Heat Transf.*, vol. 20, no. 3, pp. 408–414, 2006, doi: 10.2514/1.17713.

[34] K. Azar and C. D. Mandrone, "Effect of pin fin density of the thermal performance of unshrouded pin fin heat sinks," *J. Electron. Packag. Trans. ASME*, vol. 116, no. 4, pp. 306–309, 1994, doi: 10.1115/1.2905702.

[35] D. Lorenzini *et al.*, "Embedded single phase microfluidic thermal management for non-uniform heating and hotspots using microgaps with variable pin fin clustering," *Int. J. Heat Mass Transf.*, vol. 103, pp. 1359–1370, 2016, doi: 10.1016/j.ijheatmasstransfer.2016.08.040.

[36] H. C. Chiu, R. H. Hsieh, K. Wang, J. H. Jang, and C. R. Yu, "The heat transfer characteristics of liquid cooling heat sink with micro pin fins," *Int. Commun. Heat Mass Transf.*, vol. 86, no. June, pp. 174–180, 2017, doi: 10.1016/j.icheatmasstransfer.2017.05.027.

[37] J. Wen and Y. Li, "Study of flow distribution and its improvement on the header of plate-fin heat exchanger," *Cryogenics (Guildf).*, vol. 44, no. 11, pp. 823–831, 2004, doi: 10.1016/j.cryogenics.2004.04.009.

[38] M. Saeed and M. H. Kim, "Numerical study on thermal hydraulic performance of water cooled mini-channel heat sinks," *Int. J. Refrig.*, vol. 69, pp. 147–164, 2016, doi: 10.1016/j.ijrefrig.2016.05.004.

[39] A. A. Awais and M. H. Kim, "Experimental and numerical study on the performance of a minichannel heat sink with different header geometries using nanofluids," *Appl. Therm. Eng.*, vol. 171, no. February, p. 115125, 2020, doi: 10.1016/j.applthermaleng.2020.115125.

[40] B. Ramos-Alvarado, P. Li, H. Liu, and A. Hernandez-Guerrero, "CFD study of liquid-cooled heat sinks with microchannel flow field configurations for electronics, fuel cells, and concentrated solar cells," *Appl. Therm. Eng.*, vol. 31, no. 14–15, pp. 2494–2507, 2011, doi: 10.1016/j.applthermaleng.2011.04.015.

[41] Y. T. Mu, L. Chen, Y. L. He, and W. Q. Tao, "Numerical study on temperature uniformity in a novel mini-channel heat sink with different flow field configurations," *Int. J. Heat Mass Transf.*, vol. 85, pp. 147–157, 2015, doi: 10.1016/j.ijheatmasstransfer.2015.01.093.

[42] M. I. Pryazhnikov, A. V. Minakov, V. Y. Rudyak, and D. V. Guzei, "Thermal conductivity measurements of nanofluids," *Int. J. Heat Mass Transf.*, vol. 104, pp. 1275–1282, 2017, doi: 10.1016/j.ijheatmasstransfer.2016.09.080.

[43] M. R. Sohel, S. S. Khaleduzzaman, R. Saidur, A. Hepbasli, M. F. M. Sabri, and I. M. Mahbubul, "An experimental investigation of heat transfer enhancement of a minichannel heat sink using Al2O3-H2O nanofluid," *Int. J. Heat Mass Transf.*, vol. 74, pp. 164–172, 2014, doi: 10.1016/j.ijheatmasstransfer.2014.03.010.

[44] M. Ataei, F. Sadegh Moghanlou, S. Noorzadeh, M. Vajdi, and M. Shahedi Asl, "Heat transfer and flow characteristics of hybrid Al2O3/TiO2–water nanofluid in a minichannel heat sink," *Heat Mass Transf. und Stoffuebertragung*, vol. 56, no. 9, pp. 2757–2767, 2020, doi: 10.1007/s00231-020-02896-9.

[45] S. G. Kandlikar and W. J. Grande, "Evolution of microchannel flow passages-thermohydraulic performance and fabrication technology," *Heat Transf. Eng.*, vol. 24, no. 1, pp. 3–17, 2003, doi: 10.1080/01457630304040.

[46] A. Radwan, S. Ookawara, S. Mori, and M. Ahmed, "Uniform cooling for concentrator photovoltaic cells and electronic chips by forced convective boiling in 3D-printed monolithic double-layer microchannel heat sink," *Energy Convers. Manag.*, vol. 166, no. January, pp. 356–371, 2018, doi: 10.1016/j.enconman.2018.04.037.

[47] L. E. Paniagua-Guerra and B. Ramos-Alvarado, "Efficient hybrid microjet liquid cooled heat sinks made of photopolymer resin: thermo-fluid characteristics and entropy generation analysis," *Int. J. Heat Mass Transf.*, vol. 146, p. 118844, 2020, doi: 10.1016/j.ijheatmasstransfer.2019.118844.